

Study of onset of frost and crystals growth on hydrophilic and hydrophobic flat surfaces

by

Fuqiang Ren

A dissertation submitted to the Graduate Faculty of
Auburn University
in partial fulfillment of the
requirements for the Degree of
Doctor of Philosophy

Auburn, Alabama
May 6, 2023

Keywords: freezing time; water condensation; nucleation; contamination; ice embryo;
repeatability; fin coatings

Copyright 2023 by Fuqiang Ren

Approved by

Dr. Lorenzo Cremaschi, Chair, Director Undergraduate ResVP for Research
Dr. David Dyer, Professor of Mechanical Engineering
Dr. Roy Knight, Associate Professor Emeritus of Mechanical Engineering
Dr. Majid Beidaghi, Associate Professor of Mechanical Engineering
Dr. Nek Sharan Assistant Professor of Aerospace Engineering

Abstract

Air-source heat pump systems extract heat directly from the cold outdoor ambient and reject heat to the warm indoor environments of residential and commercial buildings. During their winter operation, the outdoor coil often accumulates frost on its surface. Frost acts as an insulator and blocks air passages, reducing the heat transfer rate and increasing the pressure drop of air passing through the coil. Defrost cycles are periodically executed in between the heating times to melt the ice, drain the water from the outdoor coil, and free accumulated frost before the heating service can start again. Unfortunately, too many defrost cycles penalize the efficiency of the heat pumps.

Currently, most research in frost mitigation focuses on superhydrophobic surfaces, lubricant impregnated surfaces, and nanostructured surfaces. Some studies proposed surface types that would lower ice adhesion such that droplets removal was promoted before freezing. However, the mitigation effects of these surfaces can be sensitive to experimental conditions and surface structure. Additionally, in circumstances where frost formation cannot be prevented due to the operating conditions, the challenge of predicting frost nucleation and growth rate is further complicated by transient flow conditions with combined heat and mass transfer phenomena to moving frost boundaries.

This dissertation presents new data of freezing time, droplet diameter, and droplet shape with different surface wettability during initial droplet icing. Water condensation and icing formed on the flat plates for convective channel flows. Four surfaces with different wettability were investigated under two test conditions. The contact angle ranged from less than 10 degree (i.e., superhydrophilic) to over 109 degree (i.e., hydrophobic). Two surfaces shared similar contact angle but had different coating components. Because frost

nucleation was partially a stochastic phenomenon subjected to many variables that were difficult to control and replicate even in a laboratory setting, frost tests with identical environmental and surface temperature conditions were repeated several times in order to gather meaningful averages for the freezing time and to quantify the magnitude of potential variability in the frost nucleation time and droplets size due to the surface wettability characteristics. The new data presented in this paper are used to inform and validate physics based frost models, which can predict the nucleation features and actual frost formation time for coated fin structures of heat exchangers. With the continually repeat experiment test for each test plate, the freezing time is not always consistent at the same test condition. Contamination particles suspended in the air and trapped on the top surface of the test plate could increase the uncertainty of the actual freezing time. Investigating the inside energy change and phase change phenomenon of single water droplets could explain the experiment results.

Combining the contamination particles with the Classic Nucleation Theory (CNT) will be used to predict the freezing time in this dissertation. The effects of contamination particles for changing the critical Gibbs energy and critical ice embryo size were discussed in this model section. Contamination particles accelerate the freezing process by enlarge the critical radius of ice embryo in the water droplet. Comparing the inconsistent freezing time results from the experiment data, the model would theoretically explain the phenomenon and give a way for onset of freezing time prediction with hydrophilic and hydrophobic flat surfaces.

Acknowledgments

I want to thank Dr. Lorenzo Cremaschi for guiding me through this Ph.D. Under his guidance, I learned how to conduct state-of-the-art research and communicate my findings to the scientific community. He helped me to grow professionally and become confident in my abilities. He also offered insight and encouragement as I learned to succeed simultaneously in my studies and new parenthood. I believe that I have grown and improved as a person because of my interactions with him over the last several years.

I want to thank my committee members and university reader; they have offered valuable insight and support to this project.

I want to thank other students in Dr. Cremaschi's lab. This study would not have been possible without the previous students' work. Ellyn Harges provided the invaluable assistance in data analysis and paper writing skills. Burak Adanur played a large part in helping me learn all the facilities and principles of experiment set up. Besides, Josh Rothe, Pratik Deokar, Stefano Morcelli, Maliha Yel Mahi, Gerard Muteba, and Jerin Ebanesar, along with the others already mentioned, worked together, Thank you for your friendship.

Table of Contents

Abstract.....	2
Acknowledgements	4
List of Tables	8
List of Figures.....	10
List of Abbreviations and Nomenclature.....	12
1. Introduction	16
1.1 Heat Pump Systems	16
1.2 Frost Growth on Evaporators.....	17
1.3 Active and Passive Methods to mitigate Frost Growth	19
1.4 Motivations of this work.....	20
1.5 Surface Coatings	23
2. Ph.D. Research objectives	25
2.1 Ph.D. Objectives overall	25
2.2 Ph.D. Approach and Scope	25
2.3 Dissertation Organization	26
3. Literature Review	27
3.1 Frost Growth on Heat Pump	27
3.2 Frost Growth on Flat Plate.....	28
3.3 Frost Growth on Hydrophilic Coatings and Hydrophobic Coatings	29
3.4 Literature review of studies that focused on measuring frost growth.....	30
3.5 Literature review of studies that focused on frost nucleation models	31
3.6 Crystals Growth Models	33

3.7 Summary of the findings from Theoretical and Analytical Studies	38
3.8 Discussion on Current Numerical Approaches to Frost Nucleation	39
3.9 Summary of Primary Observation from the Literature Review.....	39
4. Description of the Experimental Approach.....	41
4.1 Description of the Wind Tunnel Test Facility	42
4.2 Description of the Test Setup	43
4.3 Description of the Sensors and Instrumentation.....	45
4.4 Data acquisition system and controls.....	49
4.5 Experimental Procedures.....	50
4.6 Data Reduction	51
4.7 Freezing time calculation	57
4.8 Experimental Uncertainty Analysis	58
4.9 Test Plate wettability information	60
5. Discussion of the Experimental Results	62
5.1 Water Droplet size and Density	62
5.2 Measured data results and average freezing time.	65
5.3 Mass of Frost Accumulated on the Surfaces	66
5.4 Frost Thickness	67
5.5 Frost Density & Frost Thermal Conductivity	69
5.6 Repeatability of Frost Growth Process	72
5.7 Summary of the findings and lesson learnt from Experimental Work.....	76
6. Development of the Analytical model	77
6.1 Thermodynamic and Heat Transfer model.....	78

6.2 Calculation of Free Gibbs energy with ice embryo size under different Cf factor	81
6.3 Contact angle function model with different Cf level.....	87
6.4 Combine Cf factor from air contamination and substrate surface contamination.....	89
6.5 Predicted freezing time from calculated nucleation rate	91
7 Model results and comparison with the data	94
7.1 Comparison of the modeling results with data of the current work	94
7.2 Comparison of modeling results with data from the literature.....	97
7.3 Model results for relevant scenarios	102
7.4 Summary of the findings and lesson learnt from modeling efforts	106
8. Conclusions and Lesson Learnt.....	109
8.1 Conclusions from Experimental Work	109
8.2 Conclusions from Modeling Work	109
8.3 Lesson Learnt from work conducted during this Ph.D.....	109
9. Future Work.....	115
9.1 Future Experimental Work	115
9.1 Future Analytical and Theoretical works.....	115
9.1 Future Numerical Work.....	115
References	117
Appendix-Cf factor model in MATLAB code	123

List of Tables

Table 4.1: heat balance test data with all the sensible parameters	55
Table 4.2: Measurements devices, set points, ranges, accuracies, and control tolerances	59
Table 5.1: Average Freezing time and frozen droplet diameter for each flat plates and each set of test conditions.....	66
Table 6.1: Example of the model intermediate values and resulting freezing time...	86

List of Figures

Figure 4.1: Schematic of main test apparatus	42
Figure 4.2: Illustration of the HR CCD camera and IR camera with respect to the test plate	43
Figure 4.3: Image of a dew point pump and sensor device	45
Figure 4.4 T- block heat flux meter	46
Figure 4.5 Steam humidifier	47
Figure 4.6 Diagram of test apparatus with sensors positions and their distane to the leading edge of the test section.....	47
Figure 4.7 Photographic image of the visualization sensors used in the current study. (a) High Resolution Charged Couple Device (HR CCD) camera and (b) Infrared (IR) camera.	48
Figure 4.8 LabVIEW data acquisition and computer control system	49
Figure 4.9 Test Plate temperature change vs different time during the test.....	49
Figure 4.10 Calibration test 1-2ss: Heat transfer coefficient calibration	53
Figure 4.11 Calibration test 1-2ss: Surface temperature calibration.....	53
Figure 4.12 Calibration test 2-1sh: Heat transfer coefficient calibration.....	54
Figure 4.13 Calibration test 2-1sh: Surface temperature calibration.....	54
Figure 4.14 Water droplets measurement	55
Figure 4.15 Frost thickness measurement	56
Figure 4.16 IR image of droplets freezing on the cold hydrophobic flat plate (legend color scale on the right side indicates the measured temperature with the IR camera in °C).....	57

Figure 4.17: Contact angle measurement by using clear water droplets on different test plates.....61

Figure 5.1: Average droplet diameter and droplet shape on a different flat plate with a hydrophilic and hydrophobic coating. Flat Plate B ($\theta < 10^\circ$) was taken at freezing time around 7 minutes under -3.8°C (25°F) surface temperature; images for Flat Plate A ($\theta \approx 88^\circ$), Flat Plate C ($\theta \approx 108^\circ$), and Flat Plate F ($\theta \approx 110^\circ$) with coating substrate type 2 were taken around 12-13 minutes.63

Figure 5.2: Average droplet area coverage vs different surface wettability. (a) 25°F Surface temperature test condition. (b) 23°F Surface temperature test condition.....64

Figure 5.3 Cumulative frost mass during the experimental frosting test. Surface A under 41°F air temperature, 25°F surface temperature freezes at 3154 sec from beginning.67

Figure 5.4, Flat Plate B: Frost thickness growth during the test period.68

Figure 5.5 Measured frost density at three different frost layer locations.70

Figure 5.6 Measured emissivity corresponding to different frost density.71

Figure 5.7 Thermal conductivity with different frost layer thickness71

Figure 5.8: Freezing time vs. number of repeat tests for Flat Plate A ($\theta \approx 88^\circ$), Flat Plate B ($\theta < 10^\circ$) and Flat Plate C ($\theta \approx 108^\circ$) under test conditions 1. ($T_s =$

$25^{\circ}\text{F}, T_{a,in} = 41^{\circ}\text{F}, \omega_{in} = 80\% \text{ R.H.}, V_a = 3.8 \text{ m/s}$

.....73

Figure 5.9: Freezing time vs. number of repeat tests for Flat Plate C ($\theta \approx 108^{\circ}$) with coating substrate type 1 and Flat Plate F ($\theta \approx 110^{\circ}$) with coating substrate type 2 under test conditions 2. ($T_s = 23^{\circ}\text{F}, T_{a,in} = 41^{\circ}\text{F}, \omega_{in} = 80\% \text{ R. H.}, V_a = 3.8 \text{ m/s}$).....74

Figure 5.10 each freezing time at different repeat test.75

Figure 6.1 Schematic of the Pure Water Droplets to describe the modeling work of Nucleation Theory.....78

Figure 6.2 Free Gibbs energy changes with the radius of the water/ice cluster under different contamination levels.....84

Figure 6.3 F function with x for transferring heterogeneous model.87

Figure 6.4 surface tension reducing effect for free energy change.....88

Figure 6.5 Schematic for calculating the area ratio δ90

.....90

Figure 6.6 surface tension effect on ice nucleation rate.90

.....90

Figure 6.7 The ice nucleation rate changes with the different subcooled water droplet temperature.92

.....92

Figure 7.1 Predict freezing time of different surface wettability comparing the experiment test data at plate temperature 25 F.94

.....94

Figure 7.2 Predict freezing time of different surface wettability comparing the experiment test data at plate temperature 23 F.
.....95

Figure 7.3 Predicted Freezing time of two different test plate with the more than 10 repeat tests under a certain assumed Cf factor range.
.....97

Figure 7.4 literature data validation with prediction results of two different contact angle surface at -6.5°C water droplet temperature.
.....100

Figure 7.5 Free Gibbs energy change varies with radius of ice embryo under different subcooling temperature.
.....104

Figure 7.6 At different periods, water droplets contact angle has no consistent measurement.
.....105

List of Abbreviations and Nomenclature

English Symbols

A	area [m ²]
AC	area coverage [-]
c_p	specific heat capacity [J/kg-K]
F	Adjusted factor
G	Free Gibbs energy
h	heat transfer coefficient [W/m ² -K]
I_c	Current temperature nucleation rate [unit: cm ⁻³ s ⁻¹]
J	Nucleation rate [cm ⁻³ s ⁻¹]
k	thermal conductivity [W/m-K]
k_B	Boltzmann constant = 1.38×10^{-23} J/K
L	plate length in the direction of airflow [m]
m	mass [g]
\dot{m}	mass flow rate [kg/s]
Nu	Nusselt number [-]
$PM_{2.5}$	air pressureFine particulate matter 2.5 [microns]
P_v	vapor pressure [Pa]
Pr	Prandtl number [-]
q''	heat flux [W/m ²]
\dot{Q}	heat transfer rate [W]

r	radius [m]
RH	relative humidity [-]
SSD	supersaturation degree [-]
T	temperature [K]
t	time [s]
t_f	freezing time [s]
U	Chemical potential
v	molecular volume [m ³ /mol]
V	air velocity [m/s]
Vol	volume [m ³]
W	plate or channel width [m]

Greek Symbols

α	thermal diffusivity [m ² /s]
Δ	difference [-]
δ_f	frost thickness [m]
θ	contact angle [radians]
μ	Chemical potential [-]
ρ	density [kg/m ³]
ρ_v	vapor density [kg/m ³]
σ	surface tension [N/m]

i	Number of molecules
ω	absolute humidity ratio [kg/kg]

Subscripts

<i>avg</i>	average
<i>Cf</i>	Contamination factor
<i>CCD</i>	Charge-coupled device
<i>CNT</i>	Classic Nucleation Theory
<i>cond</i>	conduction
<i>conv</i>	convection
<i>dew</i>	dew point
<i>f</i>	frost
<i>s</i>	surface
<i>sat</i>	saturation
<i>sens</i>	sensible
<i>tp</i>	triple point
<i>w</i>	liquid water
<i>in</i>	Inlet of the test section
<i>out</i>	Outlet of the test section

Chapter1-- Introduction

1.1 Heat Pump Systems

Air-source heat pump systems extract heat directly from the cold outdoor ambience and reject heat to the warm indoor environments of residential and commercial buildings. The performances of these systems are dependent on the air conditions of the outdoor environments. During winter operations, the outdoor coils often accumulate frost on their surfaces. Frost acts as an insulator and blocks air passages, reducing the heat transfer rate and increasing the pressure drop of air passing through the coils. These two combined effects lead to an increase in the temperature difference between the evaporating refrigerant and the outdoor air. This phenomenon enhances frost formation and, at the same time, lowers the coefficient of performance of the heat pump. Defrost cycles are periodically executed between the heating times to melt the ice, drain the water from the outdoor coils, and free accumulated frost before the heating service can start again. Unfortunately, defrost cycles penalize the efficiency of heat pumps, and their frequency should be monitored and controlled. One potential means of reducing the number of defrost cycles is to utilize particular surface types or chemical surface coatings on the heat exchangers' fin structures.

The frost formation spontaneously occurs when surface temperature passes the dew points. The water vapor in the atmosphere condensed on the cold plate to be liquid. With the temperature continually cooling down, the liquid freezes into ice or frost. Frosting affects the performance of devices due to decreasing the overall thermal efficiency. Frost accumulated on the fin surface of heat pump can act as an insulator. It is worth investigating the frost properties and frost nucleation effects in the early stage of frost formation.

1.2 Frost Growth on Evaporators

Frost growth on evaporators is always a popular topic and discussed in previous studies. Frost thickness, onset freezing time and other frost properties are highly influenced by outdoor environments and evaporators surface itself. For outdoor environments, it mainly has two terms air quality and air parameters which include air velocity, humidity ratio and air temperature. While the evaporators have different fin structures, such as the flat surface with different wettability, coating or uncoating surface types.

For variable environmental conditions typical of heat pump or outdoor evaporator operating conditions, frost formation has three stages: the droplet condensation and growth stage, the crystal growth stage, and the frost full layer growth stage (Hoke et al., 2000). All stages are sensitive to surface temperature, air temperature, humidity ratio and air velocity. Besides these variables, droplet growth rate and onset of freezing depend on the surface wettability, at least to some extent. Tao, et al. (1993) observed frost growth consisting of two stages. The first stage was liquid droplet growth, and the second stage was ice crystal growth. The transition time between the two stages was meaningful for numerical modeling of frost formation.

Theoretically, when test surface temperature is above the dew point, only sensible heat occurs. If the surface temperature is below the dew point temperature, the water condensation will occur and freeze into a solid phase. While both surface and dew point temperatures were below 0°C simultaneously, the vapor desublimation phenomenon may occur. Further, Na and Webb (2003) pointed out the supersaturation degree (SSD) is dependent on surface energy. Supersaturation degree (SSD) is the difference in temperature between the bulk airflow and test surface. It played a critical role in droplet freezing before

entering the solid phase. Except for SSD, these stages of phenomenon also are very sensitive to air velocity and surface wettability.

Recall our experimental observation, at the certain air temperature and specific humidity ratio, the small irregular shape water droplet will condense at the cold test plate, grows gradually with time. However, the height of the droplet does not have a significant increase until the droplets freeze into the ice column structure. This whole period is called the water condensation phase. In the second stage, the ice crystal grows to act as an ice column structure, and thickness experienced a significant increase in this period. The first two stages can be highly affected by the surface status and air-side conditions. With the thickness of frost layer increasing, the third stage occurred, the frost layer will have a homogeneous growth in this period. The frost presented a porous medium shape and had a slowly increasing trend of thickness growth.

The frost layer has a porous structure consisting of ice crystals and air pores. This porous structure has low thermal conductivity; thus, it will cause a significant heat transfer resistance from the air to the evaporator surface (Na and Webb 2003). The thickness of frost layer grows on the evaporator surface and acts to block the air flow. This blockage of the air will increase the air pressure drop and reduce the air flow rate. Then the performance of the evaporator will be degraded. The air stream conditions, mass diffusion rate within the frost layer and thermal conductivity of the top frost layer needs to be well predicted to protect the performance of the evaporator for future research.

1.3 Active and Passive Methods to mitigate Frost Growth.

Because these sensitive factors highly influenced the water droplets and frost growth, it is worthy to start collecting a large amount of experimental data and develop the correlations to predict the frost delay time. The surface condition could be adjusted for delaying droplet formation and actual freezing time. The surface condition can be summarized as surface status and surface temperature. If the air always entered the test section with the same temperature and humidity ratio, the surface wettability can significantly change the droplet/frost layer and actual freezing time. So, it is worth studying the effects of surface treatment. The different surface contact angles are the main target of the surface wettability treatment. Except for the wettability of the different surfaces that could influence the droplet behaviors and frost crystal growth, other factors also can dominate the droplet formation rate and frost properties, such as the water droplets coalescence, the effect from surface segmentation, surface chemical coating, latent heat-releasing during the freezing process, and Gibbs energy change before freezing. Therefore, these interesting experimental phenomena and performing principal theory would lead us to explore future research and fill in the gaps missed from previous work.

Sheng et al. (2020) presented droplets shapes and wet area coverage on different surface types and observed that the results for superhydrophobic surfaces were different from those for a hydrophobic surface. They also indicated that droplets on a hydrophilic surface had large wet area coverage and larger water droplets. Kim et al. (2016) indicated that the radius of the droplets on a surface increased due to two droplets merging together. Hoke et al. (2000) observed that if cold substrate temperature decreased, smaller and more uniform droplets were formed. Seki et al. (1985) utilized two different test plates having

contact angles of 110° and 43° . Frost incipient phenomena showed that droplets on the 43° plate were larger than on the plate having the large contact angle. Bryant (1995) observed that a hydrophobic coating delayed the onset of ice nucleation by 15 to 35%, and the additional time allowed 15 to 25% more water condensation on the surface before the droplets froze. Adanur, et al. (2019) investigated the effect of biphilic coatings with regions of hydrophilic coatings adjacent to areas with hydrophobic coatings. Their investigation indicated that this kind of surface wettability can influence the droplet movement and delay freezing. Harges, et al. (2020) investigated the effects of surface wettability under different test conditions. The average droplets distribution and average diameter were also presented. Kim et al. (2015) had 10 repeated tests for each contact angle from 70° to 160° . The uncertainties of the frosting time of their 10 repeated tests had a maximum of 9.5%. They concluded that when test plate temperature was -12°C (10.4°F), the dimensionless freezing time increased with increasing water contact angle, while when test plate temperature was -10°C (14°F), it did not have an effect on freezing time retardation.

1.4 Motivations of this work.

Heat humps are widely used in the Southeast as the ideal solution for efficient cooling and dehumidifying as well as winter heating. Frosting formation frequently occurs in the fin located on the evaporator of heat pump to slow down the heat removal and restrain the fullest cooling efficiency. Preventing frost formation will become a crucial task for generating new type air-source heat pumps or refrigeration systems. Understanding the frost formation or onset freezing characteristics will make it easier to create a new technique for developing high efficiency heat humps which could apply in complex outdoor environment.

For investigating the frost nucleation phenomenon, high-speed camera and infrared camera is necessary to be applied in the experimental test. During the observation of whole process of frost formation, the water condensation on cold test plate or frost/ice nucleation are highly influenced by air temperature, air humidity, air face velocity, droplet temperature and surface wettability. Sahin et al (2007) experimentally studied the early stage of crystal growth by measuring the frost height, frost deposition rate, and frost density. Different parameters such as plate temperature, air temperature, air humidity ratio and Reynolds number are clarified by the uncertainty studies. Sommers et al (2016) analyzed the frost layer properties with different coating plates. Surface wettability should be included as a parameter to develop frost density in future model work. Although researchers have developed completed experiments method to investigate the air conditions and surface energy, there is still no durable technique to explain the inconsistency experiment phenomenon occurred in frost nucleation or freezing time.

Many researchers also developed early droplet condensation model and crystal frost formation model. However, few researchers developed the model on different coating test plate, which the hydrophilic, hydrophobic and biophilic surface shows the contact angle and surface tension plays an important role in onset freezing or early nucleation phenomenon. Piucco et al (2008) developed a mathematical model for the heterogeneous frost nucleation on flat surface comparing the classical nucleation theory. Then the contamination particles could be added to the surface condition concept which includes the plate temperature and contact angle. However, there are few nucleation models to show the surface contamination particles as the input in nucleation model.

Air conditions and surface conditions both affect the water droplet distribution and frost nucleation on the cold test plate. Contamination particles suspended in the air and contamination particles on the top surface of the test plate can influence the frost embryo formation and growth. No matter the natural convection test or force convection test, there are different contamination levels affecting the nucleation results. However, there is a significant gap in characterizing the contamination level in previous experimental and theoretical studies. The common practice is to neglect the contamination level when predicting the nucleation rate. Because the contamination particles are not easily controlled during the experiment test. Contamination particles suspended in the air of the wind tunnel depend on the air quality or air filter size. Except for considering the air contamination, the contaminations in the test substrate also could change the surface wettability and influence the freezing prediction. When both contamination particles in the air and metal plate both exist in the test, it will be extremely difficult to control it as constant for all repeat tests. In other words, all these contamination particles could not be neglected for predicting the frost freezing results. Although contamination particles in the air or in the substrate cannot be neglected and controlled, changing the air filter in time or applying the cleaning method after each test will reduce the effect of contaminations particles.

In this dissertation two methods were applied to improve the accuracy of the experiment frost test. Firstly, 99% isopropyl Alcohol was used to clean the superhydrophobic surface and deionized water was used to clean the super hydrophilic surface for each test. Secondly, at least 7-10 repeat tests were proceeded for each test plate to reduce the effect of contamination particles. In the beginning assumptions of the experiment conditions, contamination particles were assumed as constant for each day and

each test plate after the frosting. From the repeat experiment frost test results, the freezing time results were not inconsistent at the same test condition. By continually testing all other plates for surface wettability results, the frost freezing time results still could reach the expecting of the surface wettability. Therefore, the contamination particles might vary for each test plate and significantly influence the actual freezing time consistency in micro level. By searching the theory for supporting these inconsistency results, there is no clear theory or model for using the contamination particles predicting the frost characteristic. Previous researchers always neglected the contaminations effect for frost test, even including the beginning of assumptions in this dissertation. Heterogeneous nucleation theory may provide a strong relation for predicting the contaminations effects. Dismissing the contamination particles assumptions would give a approach for this predicting model. While this simplification could work reasonably well when predicting frost thickness on evaporators operating for a few hours, the contamination level could play an important role in the very initial few minutes of onset of frost nucleation. In addition, as will be shown later in this dissertation, the freezing time can significantly be affected by the level of contamination of the frosting surface.

1.5 Surface Coatings

Several test plates with different wettability were investigated in this research. Test plates were provided by Circle-Prosc0, Inc. The surface coating information of the test plates is shown below.

Coating Descriptions:

Alcoat®5010 - a non-chrome, non-phosphate aqueous conversion coating which is used as a replacement for chromate and iron/zinc phosphate coatings. A-5010 is used as a

pretreatment to impart improved corrosion resistance and good paint and rubber adhesion. A-5010 does not contain regulated metals, so-called “heavy metals”.

Alcoat®6000 - a non-chrome, non-phosphate aqueous conversion coating which is used as a replacement for chromate and iron/zinc phosphate coatings. A-6000 is used as a pretreatment to impart improved corrosion resistance and good paint and rubber adhesion. A-6000 does not contain regulated metals, so-called “heavy metals”. Alcoat®6000 may be selected for pretreatment applications with severe paint adhesion testing requirements.

AH-558 - a coating designed for Air Conditioning evaporators to improve water management and enhance heat exchanger cooling efficiency. AH-558 is water-based and has organic and inorganic components. The cured AH-558 coating is hydrophilic, such that when a water droplet is placed on the coating, it will spread and have a low contact angle. The AH-558 coating film becomes adherent and durable after exposure to the prescribed temperature and time cycle in an industrial oven.

AH-670 – a polymer resin based product designed to enhance heat exchanger resistance to corrosive environments. AH-670 is aqueous-based. The cured AH-670 coating is hydrophobic, such that when a water droplet is placed on the coating, it will bead and have a high contact angle. The AH-558 coating film becomes adherent and durable after exposure to the prescribed temperature and time cycle in an industrial oven.

All 6 sets were subjected to the same four steps of Surface Preparation. Each set was subjected to coating solutions, as required. Most test plates coating were prepared as several steps: mild cleaning, rinse, acid cleaning, rinse, conversion coating, rinse and oven dry.

Chapter2--Ph.D. Research objectives

2.1 Ph.D. Objective.

My dissertation presents a theoretical model that predicted the onset of frost nucleation on flat surfaces when surface energy and level of contamination are taken into consideration. The new model, which was also experimentally validated, captured the effects of surface contact angle and, more uniquely, isolated and quantified the effect of contamination of the surface in accelerating or delaying frost nucleation. The specific objectives of my Ph.D. research are as follows:

- (1) To investigate the new surface wettability performance effect on frost nucleation.
- (2) To verify frost correlations with additional data and various surface coatings
- (3) To develop a model for frozen and unfrozen phenomena in repeated frosting tests
- (4) To advance fundamental understanding of thermodynamics model for predicting freezing time.
- (5) To model frost growth on folded fins without and with louver for microchannel-type evaporators of air-source heat pump and refrigeration systems

2.2 Ph.D. Approach and Scope

My Ph.D. research included extensive experimental work and theoretical modeling. Both were required to achieve the objectives described in the previous section.

During my Ph.D. research, plenty of experimental data were taken to investigate the frost nucleation theory. My thoughts were that there must be a theory to support my observations of apparently random freezing time results from my experiments. One approach was looking at the free Gibbs energy of ice embryo, which changed during the freezing process. Specifically, the two water droplets have a sort of “chemical reaction” to

become one solid ice crystal. In this reversible process, the critical free Gibbs energy determines the maximum energy line to have the phase change and the nucleation rate will explain the frozen and unfrozen phenomena.

2.3 Dissertation Organization

The rest of this dissertation was organized as follows: In chapter Three we presented the information of literature review. Specifically, chapter three covers the previous research about the frost growth on heat pump, flat plates and different surface wettability. Excepting for covering the summary of the findings from the experimental work, the frost nucleation models and numerical approaches in the literature also were introduced in this section. In chapter four, the description of the experimental approach was present. This section includes test facilities and test setup introduction, experimental procedures, and uncertainty analysis. Chapter five presented the experimental results and lessons learnt from the experimental work. In Chapter six, The analytical model results which include the thermodynamic and heat transfer model, droplets nucleation model and Frost growth model were discussed. Chapter seven showed the model comparison with the current work and previous results from the literature. Chapter eight and Chapter nine gave the conclusions and future work.

Chapter3--Literature Review

Air condition affects the outdoor coil performance of heat pump systems. Close to 0°C and at atmospheric pressure, the frost nucleation consists of distinct stages: an initial water droplet condensation, water droplet growth to a critical size, liquid water freezing in solid ice structure, crystal frost growth and fully frost growth. For the early stages include the water condensation, water droplet growth and onset freezing process are highly influenced by air and surface conditions, that air temperature, air humidity, air face velocity, air contamination and surface energy. After the onset freezing period, the frost crystal growth and frost fully homogeneous increasing period are lightly influenced by surface conditions. These studies often reported the droplet and frost characteristics by testing on the flat plate with different parameters. Some of the nucleation theories are proved by researchers who developed model to predict the frost properties and freezing time. However, the combination of experimental test data with corresponding model could strongly predict the actual results on different surface wettability, air conditions and contamination effects.

3.1 Frost Growth on Heat Pump

Guo and Chen et al (2008) found that the COP of the heat pump drops quickly when the outdoor air temperature reaches 0 °C under different relative humidity condition. COP is the main characteristics for evaluating the performance of the outdoor heat pump. At the similar outdoor environment experimental condition, the frost growth could block the air circulation into the fins space of the heat pump. The efficiency of heat exchange will be dropped during the heat pump system. It is worth investigating the air temperature and

relative humidity effects on the COP of the heat pump system. Chung et al (2019) developed a numerical model of air source heat pump to predict the frost growth and performance of the heat pump system with different frost conditions. Many researchers investigated the frost growth and performance of heat pumps by varying different frost thickness, frost density and frost formation rate. These three parameters are the main characters for analyzing the frost growth. Based on these numerical models and empirical models, frost nucleation rate is very slow during different stages and could be observed by using high resolution camera. Xu et al (2013) used the CCD camera to understand the cycle frosting under the sample of microchannel heat exchangers. For microchannel structure in the heat exchangers, the space can be very thin around 4mm. Many researchers started to test frost formation on the microchannel structure heat exchangers for investigating its performance. Shao et al (2010) analyzed the commercial heat pump performance by comparing the microchannel heat exchangers as evaporators with using the conventional fined-tube heat exchangers. Except for the common type of different fin structures that were studied by previous researchers, the louvered fin as the new and complex structure was introduced. Xia et al (2006) presented the heat transfer and pressure drop data for different fin structures and geometries, also the overall heat transfer coefficient decreased, and pressure drop increased by varying the louvered fin. These comparison data and precious studied research is very helpful to analyzing the efficiency of the heat pump system.

3.2 Frost Growth on Flat Plate

In order to figure out the most important factors which can affect frost nucleation. Many researchers built a control test section for varying the air temperature, air humidity,

air velocity, and plate temperature. A square or rectangle shaped flat plate was installed in the test section for collecting the frost. Leoni et al (2017) tested the $30 \text{ cm}^2 \times 30 \text{ cm}^2$ aluminum plate with 1-4 m/s air velocity, 5-19 °C air temperature, 50%-80% air relative humidity and -25-0 °C plate temperature. The frost formation on the flat plate was highly dependent on these sensitive factors. Hermes et al (2009) experimentally investigated the surrounding air temperature humidity and velocity and surface temperature. They pointed out that these factors are important and sensitive to frost formation. Hoke et al. (2000) observed that smaller and more uniform droplets were formed if cold substrate temperature decreased. Yoon et al (2010) measured the frost thickness and frost mass on a flat plate. Because frost thickness grows on the flat plate is easily measured by the researchers. Same as the frost mass, all the water condensed on the flat plate and frost frozen on the flat plate can be measured or calculated. Ignoring the gravity effects for water droplets condensed at the test plate, horizontal flat plate was applied in various experiment conditions. The dew point meter could precisely capture the inlet and outlet humidity ratio to calculate the frost mass and frost density in the select area of the flat plate. Mao (1991) experimentally investigated the frost accumulation and local frost mass concentration on the flat plate under forced convection condition.

3.3 Frost Growth on Hydrophilic Coatings and Hydrophobic Coatings

Except for considering the relative parameters affecting the frost growth, the test plate surface conditions also played a significant role in the frost formation and frost growth. Surface wettability includes hydrophilic coatings and hydrophobic coatings. Different surface conditions could have large or small water droplets and different droplets shape. Sheng et al. (2020) presented droplet shapes and wet area coverage on different

surface types. They observed that the results for a superhydrophobic surface were different from those for a hydrophobic surface. The droplets on a hydrophilic surface had large wet area coverage and larger water droplets comparing droplets on hydrophobic surfaces. During the water droplets formation stage, due to the surface wettability may not be consistency for the entire plate, two water droplets could merge together which is called the coalesces. Kim et al. (2016) indicated that the radius of the droplets on a surface increased due to two droplets merging. Seki et al. (1985) utilized two different test plates having contact angles of 110° and 43° . Frost incipient phenomena showed that droplets on the 43° plate were larger than on the plate, having a large contact angle. The surface wettability can change the water droplets size especially in the early stage of the water condensation. Besides these effects, the freezing time could be delayed by varying the contact angle of the test surface. Bryant (1995) observed that a hydrophobic coating delayed the onset of ice nucleation by 15 to 35%, and the additional time allowed 15 to 25% more water condensation on the surface before the droplets froze. For other surface wettability type, biophilic coatings has combined hydrophilic area and hydrophobic area. Adanur et al. (2019) investigated the effect of biophilic coatings with regions of hydrophilic coatings adjacent to areas with hydrophobic coatings. Their investigation indicated that this kind of surface wettability could influence the droplet movement and delay freezing. retardation.

3.4 Literature review of studies that focused on measuring frost growth.

Density is an important thermodynamic property for frost because it affects frost thermal conductivity and frost thickness. Several studies in the literature measured frost

density and a comprehensive review of this topic is outside the scope of my dissertation. However, a few are reported here for completeness. Brian et al (1970), Kim et al (2002) and Hayashi et al (2007) measured frost density which range from 60-180 kg/m³. Hermes et al (2009) measured the frost density and ranged from 80 – 300 kg/m³. Kandula (2011) and Yang and Lee (2004) agreed to the experiment results. Shin. J et al (2003) recorded the frost formation in 120 minutes and measured the frost thickness, frost density and frost thermal conductivity in the different samples. They concluded that the high contact angle surface had low frost density and lower contact angle surface had high frost density. The surface energy played an important role during initial stage, but with frost accumulating on the cold plate, the effect became weaker as frost grew. Same experiment phenomenon happened in Cremaschi 's group, Fuqiang et al (2020) pointed out the inconsistent freezing results might be caused by low dependence on surface wettability.

3.5 Literature review of studies that focused on frost nucleation models.

Abundant literature exist for frost growth and a simple search would produce over 5000 hits. However, if we focus on the early stages of frost formation, only a few studies reported models and data that were closer to the type of data I gathered in my Ph.D. dissertation. Those are the studies that I considered quite relevant for my research and a brief summary of their findings is given next.

For environmental conditions typical of a heat pump operating condition, frost formation has three stages: the droplet condensation and growth stage, the crystal growth stage, and the frost full layer growth stage (Hoke et al., 2000). All stages are sensitive to surface temperature, air temperature, humidity ratio, and air velocity. Besides these

variables, droplet growth rate and the onset of freezing depend on the surface wettability, at least to some extent. Tao et al. (1993) observed frost growth consisting of two stages. The first stage was liquid droplet growth and the second stage was ice crystal growth. The transition time between the two stages was meaningful for numerical modeling of frost formation.

Some researchers investigated wettability effects on frost growth behavior but focused on how surface type affected the overall homogeneous layer. Shin et al. (2003) studied frost growth and densification on three aluminum surfaces treated to obtain contact angles of 23°, 55°, and 88°. They observed that frost thickness was low and density was high for surfaces with lower contact angles, while frost thickness was high and density was low for surfaces with high contact angles. Additionally, the surface characteristics had significant effects on frost layer properties during early frost growth, while environmental effects dominated after two hours of frosting. They developed correlations for frost thickness, density, and thermal conductivity that were dependent on the dynamic contact angle. The correlation they presented for frost mass was dependent only on time. In contrast to Shin et al.'s results, Hoke et al. (2000) reported larger frost thickness on a hydrophilic glass surface than on a hydrophobic PTFE surface. Kim and Lee (2011) studied frosting and defrosting behavior on hydrophilic ($\theta = 2.5^\circ$), bare aluminum ($\theta = 75^\circ$), and hydrophobic ($\theta = 142^\circ$) fin surfaces. They observed very similar frost thicknesses on all three surfaces up to two hours of frosting, with that on the hydrophilic surface being slightly smaller. There was more stratification when considering frost density between one and two hours of frosting. The hydrophilic surface had the densest frost layer, and the hydrophobic surface had the least dense frost layer. The frost surface temperature was nearly the same

for all three surface types. Rahimi et al. (2015) studied frost growth on a bare aluminum surface ($\theta = 78.1^\circ$), a hydrophilic surface ($\theta = 36.9^\circ$), and two hydrophobic surfaces ($\theta = 116.1^\circ, 123.9^\circ$). They observed that the hydrophilic surface had a thicker frost layer and lower density than both hydrophobic surfaces. In contrast, the bare aluminum surface had the thickest frost layer and lowest frost density of all the surface types. Hermes et al. (2018) investigated frost growth under natural convection conditions on three surface types with contact angles ranging from 45.3° to 158.9° . They presented a correlation for frost thickness, dependent on the contact angle, though this dependence was relatively small. The contact angle had a more significant impact at small frost thicknesses. Hermes et al. (2019) later studied frost growth under forced convection conditions on four surface types with contact angles ranging from 60° to 123° . In contrast to their natural convection results, they observed such a weak dependence of frost thickness on contact angle that contact angle dependence was removed from the correlation they developed for forced convection cases. The same research group (Sommers et al., 2017) observed that, under natural convection conditions, frost density on hydrophobic and hydrophilic conditions was not well predicted by a previously developed correlation from Hermes et al. (2014) that did not include the contact angle of the surface. They developed a new correlation, which included the effects of surface wettability, which described frost density much better.

Based on the above discussion, the effects of surface wettability on a frost layer's thickness and density were inconclusive and often directly contradictory between various studies. It cannot even be said that neutral contact angles produced frost behavior between those for the hydrophilic and hydrophobic extremes since Rahimi et al. (2015) observed the thickest frost and lowest density on a bare aluminum surface with a contact

angle that fell between those of the other surfaces studied. Therefore, there is still a need for additional investigation into frost growth behavior on surfaces with different wettability. In these investigations, the entire three-stage frost growth process should be considered to more thoroughly assess the effects of surface wettability on all parts of the frost layer.

3.6 Crystals growth models

Shin et al. (2003) indicated High dynamic contact angle surface has high frost density and low frost density. It has irregular and rough crystals. In comparison, the low dynamic contact angle surface has a uniform and regular crystal, and low frost thickness, and high density. Armengol et al. (2016) developed a mathematical model for frost growth in two dimensions. They found larger thermal conductivity values in the leading edge and lower values in the rear part of the layer. Frost grows faster in the leading edge than in the rear region, in accordance with the so-called entrance effect. The leading edge has larger gradients of humidity and temperature compared with the rear region's gradient values. Sheng et al. (2020) measured the amount of condensate drainage in split fin, and louvered fin, the comparison of different air velocities and the number of fins impacted the results. Moallem et al. (2012) found that for the parameters, such as density, air pressure drop, thickness, heat capacity, and water retention, the surface temperature has a significant effect on microchannel coil frost growth, while surface wettability has a negligible effect. They also indicated the frost structure and distribution on the leading edge and inside the fin are different, influencing the frosting time. Wu et al. (2003) found the onset frost melting effect during the full frost growth period. They also indicated that multiple step occurred during the frost growth period can be caused by high air temperature and higher

relative humidity, or higher air velocity or melting effect. Yang et al. (2005) concluded that the frost surface temperature calculated from the turbulent model is higher than that from laminar flow. The effect of air velocity on the mass flux was not significant under turbulent flow, whereas the frost thickness under laminar flow increased with air velocity. Na et al. (2003) concluded that the inhomogeneity of the surface energy caused a heterogeneous frosting pattern because the required supersaturation degree for the nucleation locally differs. They also mentioned their work suggests the possibility of developing surfaces that delay frost formation to lower surface temperature. Hermes et al. (2019) used the contact angle in semi-empirical models to predict an overall frost layer's characteristic. The contact angle is the primary parameter related to surface wettability which affects frost growth.

Webb et al (2003) indicated that ice crystal could be summarized at different shapes. The thermal conductivity of the frost layer is influenced by the heat conduction paths through the ice phase. The density of the frost layer is also dependent on the ice crystal shapes. From many previous researchers, Hayashi et al, presented the mechanism of frosting during the early stage on a cold plate had different frost growth because the nucleation is strongly related to the surface characteristics. Therefore, the nucleation phase and different ice crystal structure had different properties, such as density, emissivity, and thermal conductivity. Shin, J. et al (2003) measured the frost layer thickness and calculated the frost thermal conductivity. They found that different contact angle surface had different frost thermal conductivity. The different surface energy will have different frost density which could lead to different frost thermal conductivity range from 0.06 to 0.16 W/(m K). Also with the thickness increased, the frost thermal conductivity can increase to around 0.2 W/(m K). But there are still many researchers who ignore the nucleation phase.

Yancheshme et al (2020) found that higher thermal conductivity enhances the droplet explosion process and thermal conductivity controls the released heat during the freezing of a droplet. Higher thermal conductivity causes faster freezing and a greater driving force for ice bridge growth.

B.T. Marinyuk (1980) used the frost surface emissivity 0.92 to calculate the total heat transferred as latent heat in their theory. Hermes et al (2008) assumed the frost surface to be a diffuse gray body with an emissivity of 0.9. Kwan-Soo Lee, et al (1997) applied the digital micrometer to measure the frost thickness. The temperature at the frost surface is measured by using the infrared radiation surface temperature detector by constant emissivity of frost surface is 0.94. Dozier et al (1982) presented a model to determine an all-wave emissivity of snow. All grain size of snow range between 0.985 - 0.990. They also precisely pointed out for fine grain snow, the emissivity slightly decreased to 0.985.

Tao et al. (1993b) modeled the frost layer during the crystal growth period to be a forest of growing circular fins. It focused on the growth of individual ice columns rather than on the growth of a homogenous layer. It did not include frozen droplets, though the authors mentioned that the crystals grew at the liquid nucleation sites. Instead, this model required initial thickness, diameter, temperature, and crystal distribution to begin calculations. This model assumed different temperatures for the frost crystals and the neighboring air voids, with the average temperature at the frost surface falling somewhere in between. This model was capable of transitioning to a frost layer growth model (also developed and presented in the same paper) but needed the transition time to be a model input. The overall crystal growth/frost layer growth model was compared to experimental data with surface temperatures of -10 and -20 °C, with promising results.

The second model, developed by Sahin (1995), depicted the frost layer as identical cylindrical frost columns, which grew straight up from the cold surface. Unlike Tao's model, this model treated frost during crystal growth more as a homogeneous layer since heat and mass transfer were based on an average frost temperature. It was assumed that the frost columns and air voids were at the same temperature for a given point in the frost layer. As in frost layer growth models, diffusion mass flux led to an increase in column radius (leading to densification), and the remaining mass flux increased column height. The only empirical constant used was a volumetric ratio of crystals in the overall frost layer. No mention was made of the dimensions of the corresponding columns. The model was validated using the author's measured frost thickness data between 10 minutes and 100 minutes of testing. The most significant deviations occurred at very early and very late stages of frosting.

These two models were the only existing comprehensive models found in the current investigation that described the crystal growth frosting stage in particular. Shneider (1977) used a needle structure to describe the frost layer, and Cheikh and Jacobi (2014) used a hexagonal crystal structure to obtain a mass transfer conductance term for their overall model. However, both of these models' primary focus was to predict an overall homogeneous frost layer's behavior. These models were intended to be used as stand-alone models with no need to transition to any other model format. Additionally, Ismail et al. (1997) and Tahavvor and Yaghoubi (2009) included the crystal growth stage in their model for frost growth on cylindrical tubes. They utilized Tao's modeling format rather than developing a new method to describe crystal growth. There is still lacking a crystal growth

model in which frost crystals deposit on top of frozen droplets, and which can serve as a bridge between the droplet growth and frost layer growth stages of frosting.

3.7 Summary of the findings from Theoretical and Analytical Studies

Yao et al. (2020) had two kinds of phenomena after droplet impinging on the cold surface: unfreezing and delayed freezing when the surface temperature was -10 C and -15 C. Also, they indicated the uncertainty of the freezing delay time was considerable; sometimes, the droplet would not freeze and stay in a supercooled liquid state for a long time. According to their discovery, our research also had the same issue, the uncertainty of freezing time was considerable. In our cases, the unfreezing phenomena were observed on some particular surfaces under the same test condition. Kim min-Hwan et al. (2017) presented the freezing delay time with 100 sessile water droplets under the same test conditions. They found a random distribution of freezing delay times in the range of 50-400s and 100-1250s on bare and superhydrophobic surfaces. Castillo et al. (2021) summarized the freezing process into four steps: (1) ice-embryo nucleation, (2) recalescence, (3) solidification and freezing, (4) cooling of the frozen droplet. Many groups found the latent heat was released during the solidification process. Voulgaropoulos et al. (2021) believed the freezing process of water droplets belongs to the Stefan problem involving a moving solid-liquid interface driven by heat transfer. Zhang et al. (2017) concluded that the larger supercooling degree causes a significant difference in freezing rate and time comparing without consideration of supercooling model. They believed the lower cold plate temperature or larger supercooling degree gives a higher freezing rate and shorter freezing time. Chu et al. (2017) found that with lower surface temperature, the

condensation phase driving forces became larger, resulting in a more significant droplet growth rate. The Gibbs free energy equation also was applied. Chu et al. (2017) created a regional map to classify difference droplet coalescence. Harges et al. (2020) investigated the different cleaning methods for cold test plate can cause different droplet behaviors. PM2.5 was also the primary contaminant that might have deposited on the test surfaces. Gong et al. (2017) showed that the greater the PM2.5 concentration, the thicker and greater the frost crystal.

3.8 Discussion on Current Numerical Approaches to Frost Nucleation

Blake and Thompson et al (2015) used the simulation strategy to study what surface types are best for icephobicity and how droplet diameter affects icing behavior. Niedermeier et al (2011) suggested stochastic nature of heterogeneous ice nucleation experiments should be performed if concerning the chemical composition and air contamination particles changed the air surface condition. Pruppacher et al (1995) computed the energy transferred of water molecules across the ice-water interface by using the classical nucleation rate equation under physical property data for supercooled water conditions. Chaudhary et al (2014) believed the freezing of water droplets is a heat transfer process. And their numerical modeling determined the ice fraction at the beginning period of the freezing process by investigating the energy balance. Zhang et al (2015) used the numerical simulation to prove the contact angle strongly affects the freezing process for the anti-ice/frost mechanism.

3.9 Summary of Primary Observation from the Literature Review

Many researchers investigated the frost characteristics and droplet onset freezing process by using the high-resolution camera. These raw video data provides a strong measurement for water droplet size, water droplet distribution, onset freezing time, frost

thickness and frost nucleation rate. These measured data could be affected by different surface wettability, surface temperature, air temperature, air humidity and air face velocity. A few researchers also observed the droplets coalescence effect on droplet growth or distribution on the cold test plate. Apart from analyzing these parameters effect, many researchers reported that the frost formation can be summarized as several stages. Initial water droplet nucleation, water droplet growth, water onset freezing, frost crystal growth and frost fully growth period. Besides, there are also surface wettability comparing test in the literature, superhydrophobic surface normally have large water droplet size and higher frost thickness, while superhydrophilic surface smaller water droplet diameter and lower frost thickness. Also, the frost density can be distinct from the two different surface wettability. However, few researchers recorded the actual water droplet freezing time. During the experiment test, under the same test conditions it is still difficult to guarantee the consistency of freezing time results. Because there must be an important parameter missing which could influence the onset freezing process. Except the contact angle or surface roughness affect the surface energy between the liquid water droplet to solid cold plate, the contamination particles suspended in the air and contamination particles attached on the top test plate surface could change the current surface tension and actual freezing results. Therefore, it is necessary to fill up the gap in the literature to predict the freezing time of frost nucleation and nucleation rate.

Chapter 4-Description of the Experimental Methodology

The experimental methodology of my PhD research was based on previous work from my advisor research group (Cremaschi et al., 2018). However, my research measured new data of droplet growth and freezing characteristics during initial frost nucleation. The center regions of the test plates were visually recorded by an in-situ calibrated non-invasive infrared thermal camera to provide instantaneous measurements of droplet diameter and droplet area coverage, as well as droplet freezing time. The IR camera also measured the frost surface temperature while the test apparatus measured the instantaneous heat flux and water mass deposited on the cold flat plates. With respect to authors' previous study (Cremaschi et al., 2018), the static contact angle of flat plates was extended and ranged from less than 10° (i.e., superhydrophilic) to over 109° (i.e., hydrophobic). Because frost nucleation was partially a stochastic phenomenon subject to many variables that were difficult to control and replicate even in a laboratory setting, frost tests with identical environmental and surface temperature conditions were repeated several times in different days and sometimes different months. This approach quantified the effect of surface coating robustness, that is, coating potential deterioration and/or surface potential oxidations due to multiple frost and defrost processes, cleanups, and water drying procedures. Averages and distributions of the experimental results are discussed in this paper. The variability of the frost nucleation time and droplets diameter at the onset of freezing are also presented and analyzed based to the surface wettability characteristics of new coated surfaces.

4.1 Description of the Wind Tunnel Test Facility

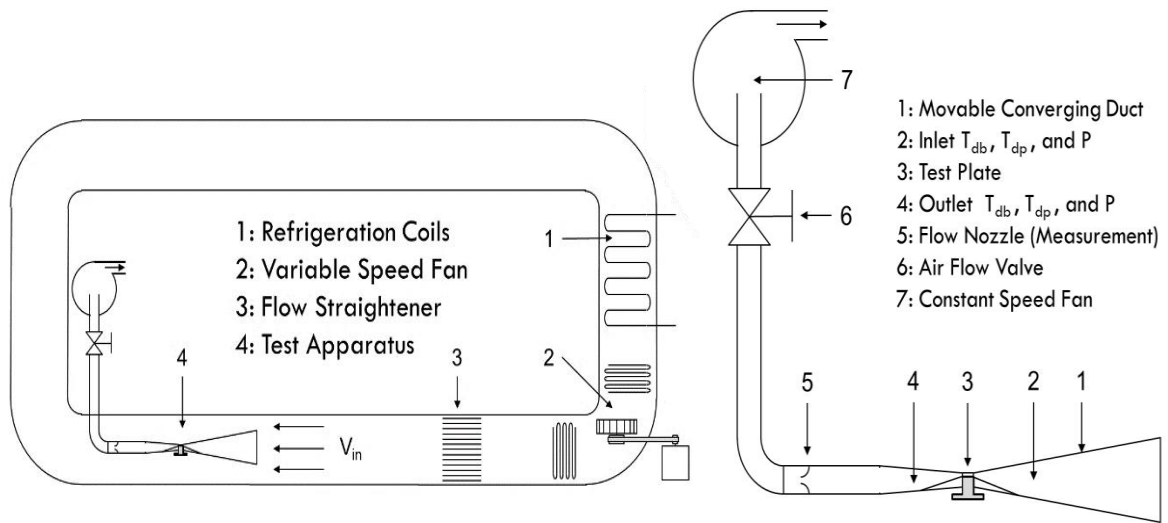


Fig. 4.1: Schematic of main test apparatus

The test facility consisted of a closed airflow wind tunnel that controlled the air temperature, humidity, and speed. The refrigeration coils were controlled at around 33-36 F by adjusting the air heater near the coils. The cold moisture air was circulated inside the wind tunnel and go through the air filter until to the test section. The variable speed fan was set around 1000 cfm to blow the air. The air face velocity to the test section will be controlled at 5 m/s or 2.5 m/s. In order to reach a high air relative humidity and purity air to the test plate, the additional humidifier was used to booster the moisture to the test window. The relative humidity, dry bulb air temperature, dew point temperature, air face velocity and test plate temperature were recorded by the DAQ device.

4.2 Description of the Test Setup

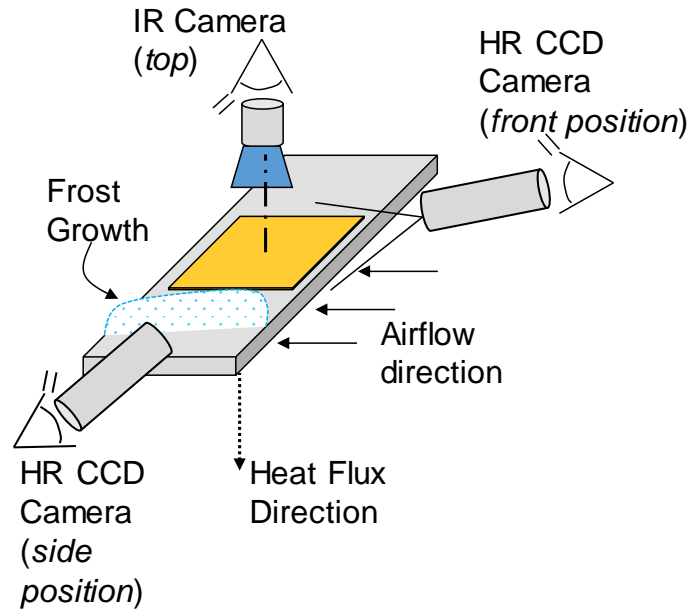


Figure 4.2: Illustration of the HR CCD camera and IR camera with respect to the test plate.

The experimental facility, test setup, sensors, and data reduction are described in detail in the authors' previous work (Adanur et al., 2019). They are briefly summarized next for completeness of this paper. In addition, the cleaning and drying procedures used during the tests were described in detail in Harges et al. (2020).

A second smaller airflow wind tunnel, shown in Figure 4(a), was installed inside the large wind tunnel, and it accommodated the cold flat plates. Two thermoelectric coolers (TECs) and an in-house built stainless-steel heat flux meter controlled the test plates' surface temperature during frosting. An infrared (IR) camera was positioned at the top of the plate, and a High Resolution Charged Couple Device (HR CCD) camera was located at the front or, in repeated tests, at the side of the test plate as shown in Figure 4(b). The IR camera measured the temperature of the frost surface and droplet size during freezing, while the HR CCD camera measured droplet size right after freezing and subsequent frost

thickness. Sensors of the test apparatus shown in Figure 4(a) measured the time-dependent heat flux, surface temperature, air dry bulb, and dew point temperatures at the inlet and outlet of the test plates, airflow rate, and air static pressure and air pressure drop across the channel of the test plate. We installed smoothly converging and diverging duct sections at the inlet and outlet of the test plate, keeping the angles low enough to reasonably assume the air flow over the plate to be initially well mixed and fully developed. These converging and diverging sections to and from the test plate sections are indicated in Figure 4(a). Aluminum plates were machined to dimensions of 25mm length (i.e., depth of the plate along the airflow direction) by 152 mm width and 6 mm thickness (1 in x 6 in. x 0.25 in). These plates are referred to as the “test plates” throughout this paper. The test plates were exposed to convective airflow frosting conditions on their top surfaces with air flow cross-section dimensions of 4 mm high (perpendicular to the surface) and 152 mm wide (equal to the width of the test section). Air entered the test plates at 5°C (41°F) dry bulb temperature and the dew point temperature was 2°C (35.5°F), which yielded an entering relative humidity of about 80% and absolute humidity of 0.0043 kg-water/kg-air. In order to maintain the dew point temperature constant at the inlet, a humidifier was utilized with purified deionized water (Water, ACS Reagent Grad, ASTM Type I, ASTM Type II). The airflow rate (4.9 CFM) was constant for the entire test, that is, during both phases of frost nucleation and subsequent frost growth. During a frost test, a nitrogen displacement technique was used to produce ultra-low dew point temperatures in the gas surrounding the test plate during the temperature pull-down period of the test plate. This nitrogen blanket avoided water vapor condensation (and frost nucleation) during the pull-down phase of the test. Then, when the test plate temperature reached the setpoint, nitrogen gas was removed,

and the air was immediately circulated onto the test plate's top surface. Water vapor condensed on the test plate surface, and droplets gradually grew. The surface temperature was constant during droplet growth, crystal growth, and frost growth stages, and the freezing time and freezing period were clearly identified from the start of the water vapor condensation.

4.3 Description of the Sensors and Instrumentation



Figure 4.3: image of a dew point pump and sensor device.

The dew point meters inlet and outlet were connected with the small wind tunnel to measure the air temperature, air pressure and dew point temperature. With these raw parameters, it will automatically show the inlet and outlet humidity ratio. Also, the ω_1 and ω_2 can be used to calculate the water mass accumulated on the test plate.

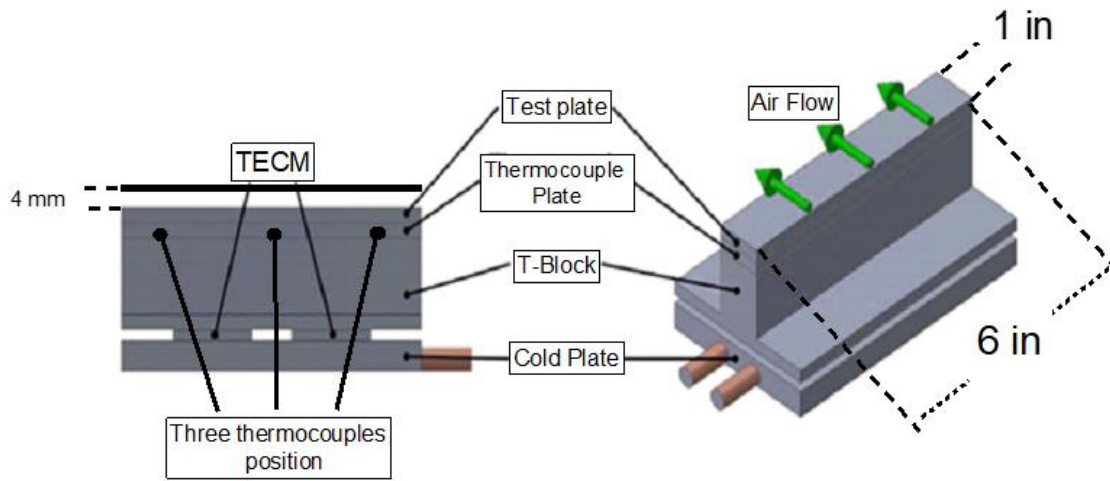


Figure 4.4: “T-block” heat flux meter

Figure above, shows the cooling device of the test plate. In the very beginning of the test period, all the in-house built stainless-steel part and Ethylene glycol were set at the wind tunnel stand-by temperature. After the test start, the Ethylene glycol which circulating the bottom of the T-Block is cooling down to act as a heat sink. The heat was removed from the top cold test plate to the bottom copper tube. Thermocouples were installed under the test plate to measure the plate temperature. Also, the two thermoelectric coolers (TECs) connected with the T-block and Ethylene glycol cold plate were controlled by the Data Acquisition (DAQ) systems. The two thermoelectric coolers (TECs) operate by the theory of Peltier effect. They create a temperature difference by transferring heat between two electrical junctions. The Ethylene glycol (32°F) comes from the chiller was maintained at the required constant temperature during the whole test. Figure 4.4 also provided the airflow cross-section dimensions of 4 mm high (perpendicular to the surface) and 152 mm wide. Three T- type thermocouples were evenly embedded in the thermocouple plate and used to record the surface temperature during the experiment.



Figure 4.5: Steam humidifier.

The figure 4.5 above shows the steam generator to the test section. An additional steam booster was installed to give the extra humidity to the test plate. The deionized water was used to create pure steam. A humidifier was utilized with purified deionized water (Water, ACS Reagent Grad, ASTM Type I, ASTM Type II). The continuing moisture air was blowing to the cold test plate after the test start.

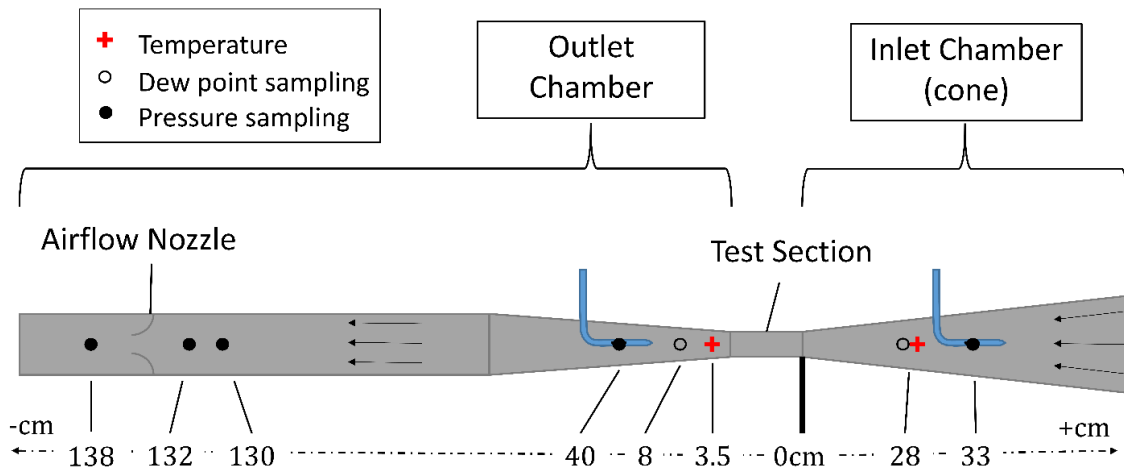


Figure 4.6: Diagram of test apparatus with sensor positions and their distance to the leading edge of the test section

In figure 4.6, The temperature calibration bath device provides accurate thermocouples for the test use. Optima High Precision Balance was used to measure the total water/ice mass accumulated on the test plate after the test. These multiple measurement instruments make sure the test system has the accurate results. Sensors of test apparatus measured the surface temperature, air dry bulb and dew point temperatures at the inlet and outlet of the test section. The airflow rate, air static pressure and air pressure drop across the channel of the test plate were also measured.



Figure 4.7: Photographic image of the visualization sensors used in the current study. (a) High Resolution Charged Couple Device (HR CCD) camera and (b) Infrared (IR) camera.

In figure 4.7, the videoscope device observes the front edge of the test plate during the whole test. The video raw data can be provided to measure the frost growth rate and frost thickness. The infrared thermal camera is located above the test plate to observe the water droplets formation and temperature range during the specific emissivity range. The video film recorded from the IR camera was used to measure the water droplets diameter and temperature change of the water condensation on the plate.

4.4 Data acquisition system and controls

Labview acted as the engineering research programming software and was used for monitoring, measuring and automatic controlling. With building the wind tunnel instruments embedded with the DAQ system, the labview will record the data signals from the experiment set-up and all other sensors. Besides the precise calculation and measurement for the test data from labview, it also gives a safety controlling for all the relative parameters of the lab instruments or equipment. Temperature, pressure, and High voltage shut down system will be ensured with a safety operating environment.



Figure 4.8: LabVIEW data acquisition and computer control system

4.5 Experimental Procedures

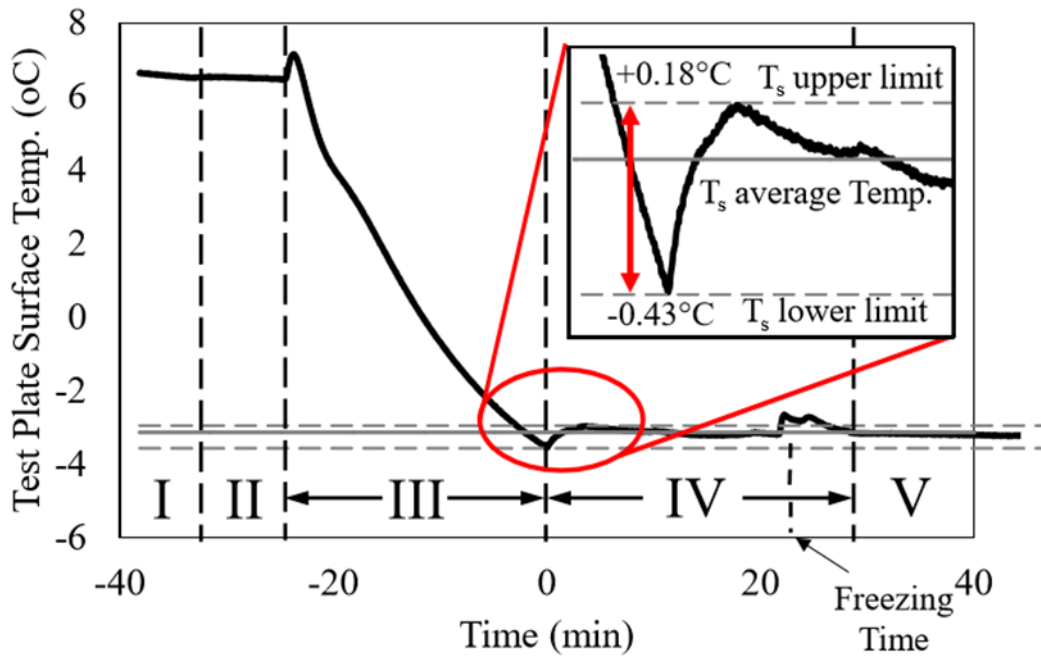


Figure 4.9: Test plate temperature change vs different time during the test

The experiment procedures can be summarized as 5 stages. The first stage is test preparation. The air temperature and air velocity need to be stable in equilibrium state. Also, during the preparing state the humidity ratio needs to reach 82% in the beginning. In the second stage, the Ethylene glycol flowed into the heat flux meter to cool down the test plate and heater of the Ethylene glycol will be on to maintain the temperature of the test system. In this stage the test plate temperature starts to drop from starting point 41°F in the wind tunnel. Now entering the third stage, Nitrogen gas will fill in the isolated test system to replace the natural air. The reason for replacing the air to Nitrogen is trying to make sure the test plate dry before droplets nucleation start. The second reason for filling in the Nitrogen is cooling down the test plate to lower temperature. The fourth stage is stopping the Nitrogen and opening the air fan. The moisture air blow into the system and small water droplets starts to condense at the cold plate. The water droplets grow rapidly until they

reach the max barrier to freeze. During the water droplets freezing process, the temperature rises significantly and then decreases to a stable range. The fifth stage is the frost full growth. Normally the video will be recorded one hour before turning off the experiment.

4.6 Data Reduction

In order to check the heat balance of the test system and installation of the test plate, it is worthy to do calibration test before the frost test started. There are two similar tests conditions to check the heat transfer coefficient of the system and Plate surface temperature. At certain Q of the Tee block under the test plate, the inlet air temperature, inlet humidity ratio and air face velocity are controlled as constant. There are many calibration tests to create the trend line for checking the heat transfer coefficient h and surface temperature T_s . See Figure 4.61, because of the operator's error during the test, it has different Q tee for every repeat calibration test. For a certain Q of the tee block in one test, the heat transfer coefficient h corresponded should be in the trend line. In the Figure 4.61 1-2ss, the two dot out of the trend line above which shows $139 \text{ W/m}^2\text{-K}$ is a good example to prove the test plate installation is not good. It gives a warning for heat balance is not equilibrium which needs to repair the leakage or rubber insulation of the test system. The three red color dots in the figure prove the perfect test condition and trustful heat balance of the system. The difference of figure 4.61-1sh is the air temperature. 1sh calibration test uses the high air temperature range and high power of the tee under the test plate. These two calibration tests normally will last one hour to completely become steady state. After the test plate surface temperature became very steady in 10 minutes, the test will be stopped. The following equations for analyzing the data will be discussed.

$$h = \frac{Q_{air}/Area}{(T_{air}-T_{surface})} \quad (4.1)$$

$$Q_{air} = \dot{m} \times (h_{in} - h_{out}) \quad (4.2)$$

$$Q_{air} = Q_{sensible} + Q_{latent} \quad (4.3)$$

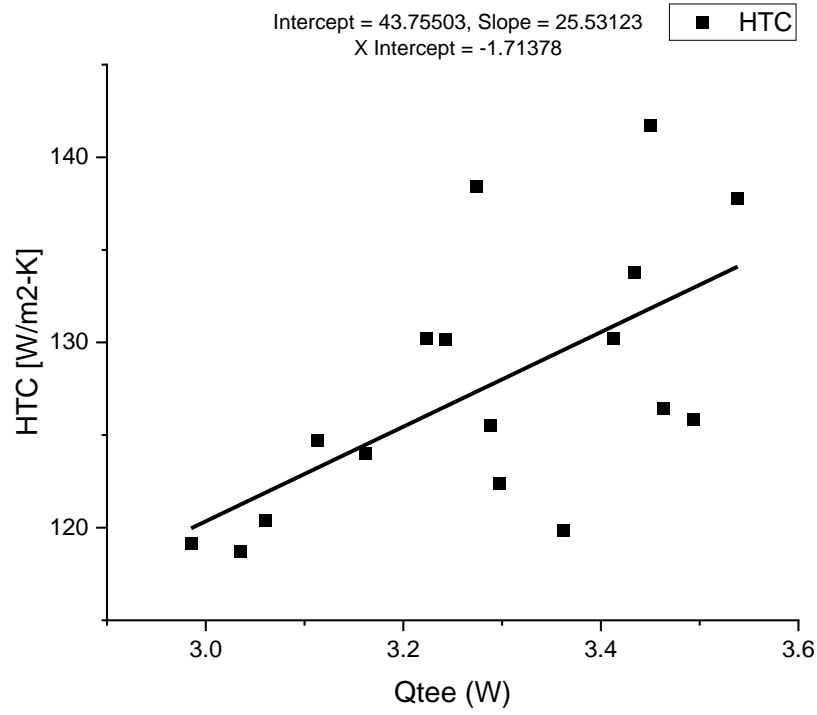


Figure 4.10: Calibration test 1-2ss: Heat transfer coefficient calibration

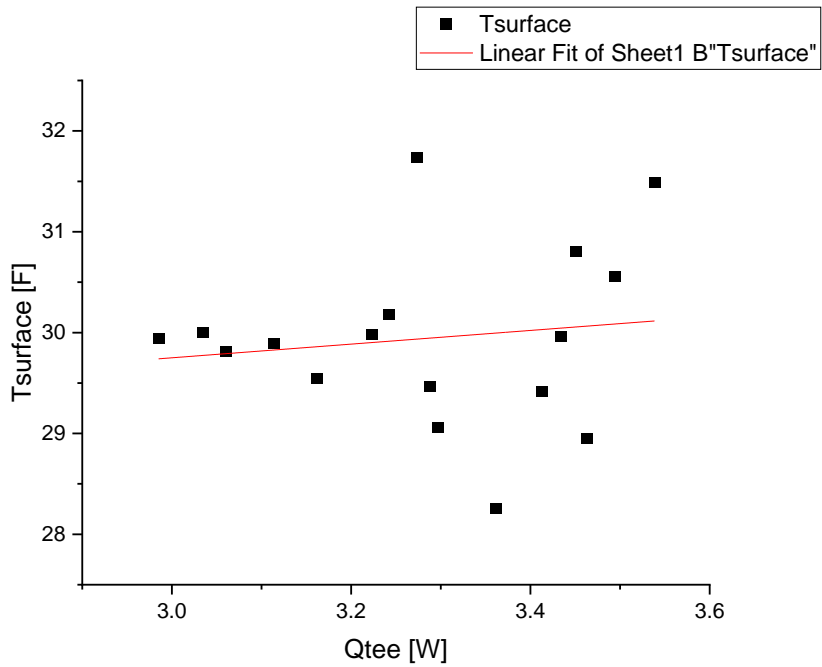


Figure 4.11: Calibration test 1-2ss: Surface temperature calibration

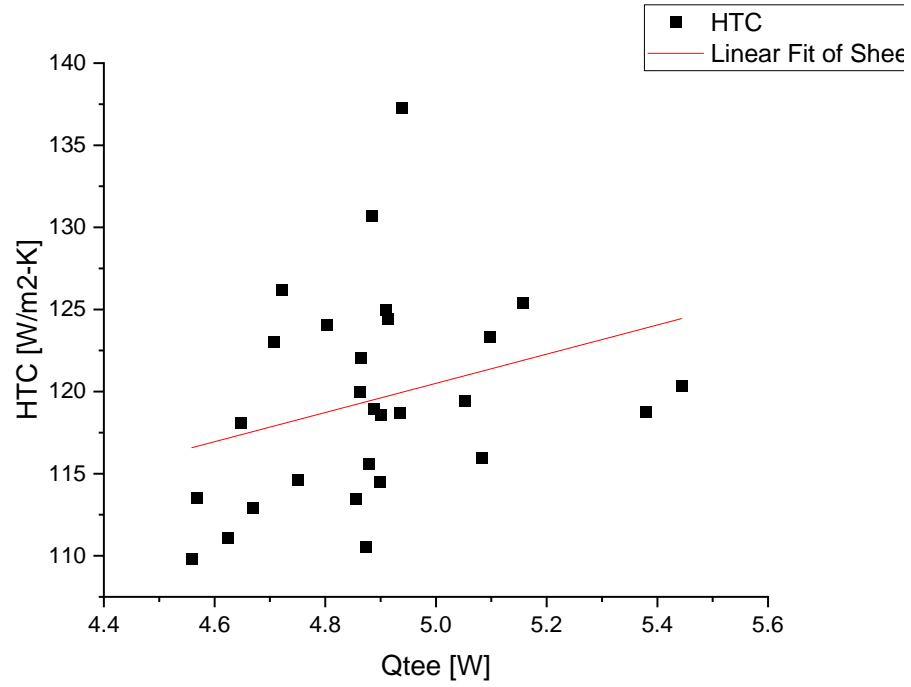


Figure 4.12: Calibration test 2-1sh: Heat transfer coefficient calibration

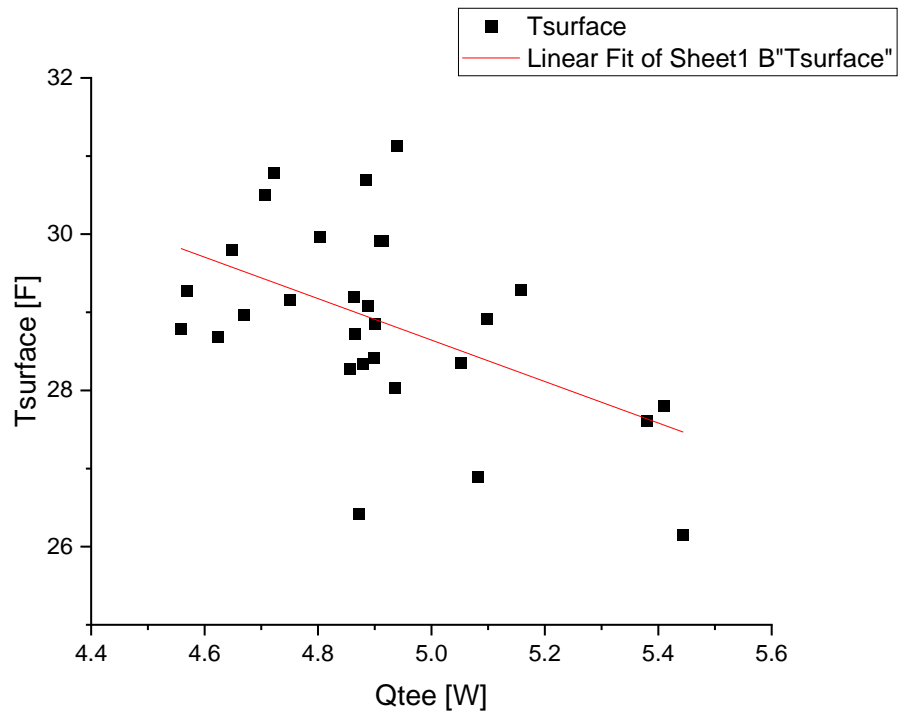


Figure 4.13: Calibration test 2-1sh: Surface temperature calibration

Table 4.1 heat balance test data with all the sensible parameter

Surface1	T _{air,in} [F]	T _{air,out} [F]	T _{surface} [F]	T _{ETW,in} [F]	T _{ETW,out} [F]	Q _{tee} [W]	Q _{gain} [W]	Heat Transfer - Air Side [W] (Enthalpy)
1sh	47.19	45.99	30.79	28.45	63.83	4.72	0.27	2.74
1sh_Surface1	47.28	46.30	30.69	28.42	62.76	4.88	0.22	2.68
2ss_Surface1	42.31	41.76	31.74	27.70	62.18	3.27	0.16	1.83
1sh_Surface1	47.30	46.58	31.13	28.54	63.71	4.94	0.16	1.91
New adjustment on System								
1sh_Surface1	47.24	46.45	29.27	28.66	62.28	4.57	0.18	1.98
2ss_Surface1	41.46	40.90	30.00	28.03	60.94	3.03	0.11	1.26

The table 4.1 lists the accuracy specifications for steady state test before frost test started. It shows the additional test to verify the heat balance of the test system prior to the frost test start. It also gives a checklist for frost test when the limit water droplets or ice condensed on the cold plate.

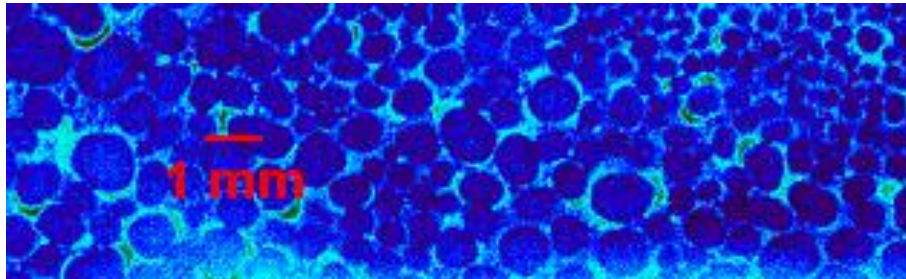


Figure 4.14: Water droplets measurement

The video from the IR camera was paused for screenshot picture. The picture was loaded by image software Image J. At the selected region of this image, the number of pixels for one water droplet can be counted as the area. The average diameter of water droplet can be calculated and measured by accounting pixels number. Except measuring the droplet size, this technology also can measure the wet area distribution on the selected area of the plate.



Figure 4.15: Frost thickness measurement

The frost thickness measurement can be used as the same method as droplets. The hand drawing tools will be applied to sketch the contours of ice crystal shape. On the toolbar of ImageJ select the line tool. Hold down the shift key and draw a straight line along the length of the scale bar of the image being as precise as possible. This is going to be the known distance that we use as a standard to set the measurements. Frost thickness also can be used to calculate the growth rate during the whole test.

4.7 Freezing time calculation

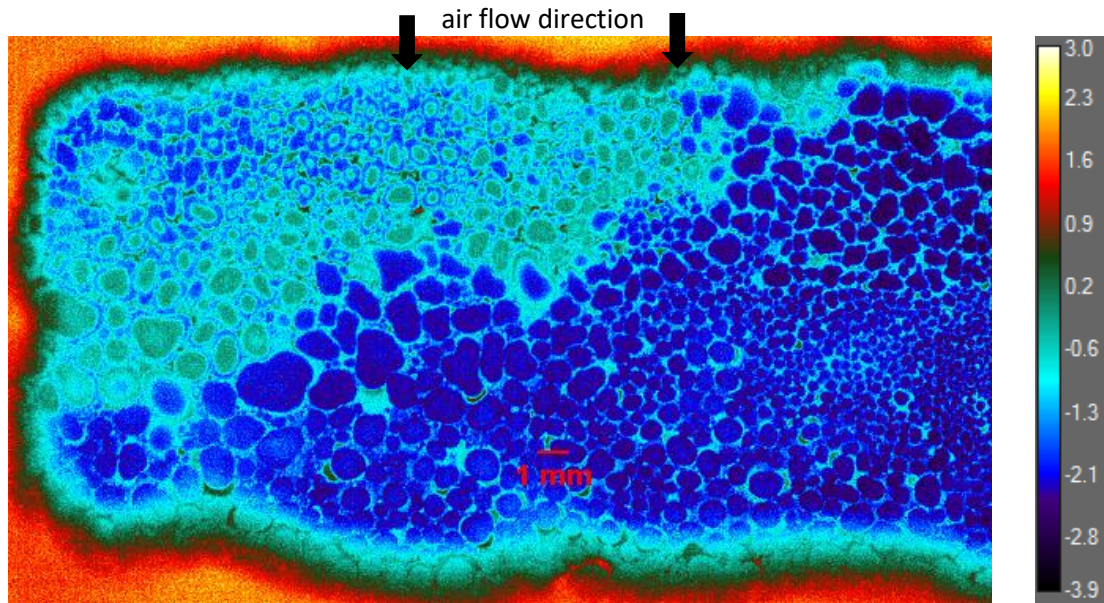


Figure 4.16: IR image of droplets freezing on the cold hydrophobic flat plate (legend color scale on the right side indicates the measured temperature with the IR camera in °C).

The change in color of the droplets determined the freezing time and freezing duration. In figure 4.16, the emissivity of the infrared camera was used for checking the relative readings from the thermocouples before, during, and after the frost developed on the surface. The absolute temperatures measured from the IR camera was not used for any of the data reduction methods, as discussed in the previous section. However, the relative change of color from dark blue to light blue coincided with the freezing time reported by a “spike” in the surface temperature profile in figure 4.9. Thus, the relative change in color of the water droplets detected by the IR camera represented that phase change from liquid to solid. This was helpful when estimating the start (t_1) and end (t_2) of the freezing period for all the droplets deposited on a surface, as indicated by Equation (1).

This single image of the freezing process in Figure 4.16 had an actual freezing time of about 12 minutes (± 0.5 minutes due to human error), and it was calculated by using equation (1).

$$t_{Freezing} = (t_1 - t_0) + \left(\frac{t_2 - t_1}{2}\right) \quad (4.4)$$

An example for calculating the freezing time of Figure 4.71 is shown as below:

The time t_0 can be defined as the time for water nucleation first occurs on the cold test plate from the beginning recording. That also can be called test start time.

The time t_1 can be defined as the first time for any water droplets turn to solid phase. The ice fraction in this freezing droplet will reach the maximum barrier to cause it to freeze rapidly.

The time t_2 can be defined as the last droplet on the test plate became solid phase from liquid phase. The freezing duration time is calculated as $t_2 - t_1$.

$$t_{Freezing} = (1642 - 920) + \left(\frac{1644 - 1642}{2}\right) = 724 \text{ s} = 12 \text{ minutes} \quad (4.5)$$

Since the IR camera captured images every two seconds, there was often only a single image of the freezing process for tests on these surfaces.

4.8 Experimental Uncertainty Analysis

Twenty T-type thermocouples were embedded in the metal block underneath the test plate to measure heat flux and to derive the plate top surface temperature. The accuracy of the sensors is reported in Table 4.2, and the authors' previous work reported more details about the instrumentation (Cremaschi et al., 2018).

Table 4.2: Measurement devices, set points, ranges, accuracies, and control tolerances

Parameter Measured	Measuring Device	Calibration	Set Point/Range	Accuracy	Control Tolerance
<i>Sensors for controlled variables</i>					
Air Temp. (dry bulb)	Thermocouple (grid)	In situ*	5°C (41°F)	±0.056°C (±0.1°F)	±0.28°C (±0.5°F)
Air Temp. (dew point)	Chilled Mirror Dew Point Meter	Manufacturer	0.56°C (~33°F)	±0.28°C (±0.5°F)	±0.28°C (±0.5°F)
Plate Temperature	Thermocouple (grid)	In situ*	-15°C (~5°F)	±0.04°C (±0.07°F)	±0.28°C (±0.5°F)
Air Volume Flow Rate	Flow Nozzle	Manufacturer	8.5 m ³ /h (~5 cfm)	±0.05 m ³ /h (±0.03cfm)	±0.09 m ³ /h (±0.05 cfm)
<i>Measured Variables</i>					
Air Pressure Drop	Pressure Transducer	Manufacturer	0 to 250 Pa (0 to 1" H ₂ O)	0.25% full scale	(-)
Frost Surface Temperature	Infrared Camera	In situ	-22°C to 5°C (-8°F to 41°F)	±2°C (±3.6°F)	±1.6°C (±3.5°F)
Frost Mass	High Precision Digital Scale	Manufacturer	0 to 5 g (0.011 lbm)	±0.1 mg (±0.0015 gr)	(-)
Frost Thickness	CCD Camera	In-situ	0.2 to 3 mm	±80 μm @ 0.4 mm ±40 μm @ above 1 mm	
Heat Transfer Rate	Conduction side	In situ*	5 to 8 W (17 to 27.3 Btu/hr)	15%	(-)
Contact angle	CCD drawing tools	In situ*	0° to 180°	±8%	(-)
*Temperature bath and temperature sensor with accuracy of ±0.05°C (±0.1°F) were used for on-site calibration.					

4.9 Test plate wettability information

The test plates were rectangular bars of about 6 mm (0.25 in) thickness. Four substrates and different coatings were developed, and the main body of the plates was 6061 Aluminum. While the specific details of the coating's composition are of proprietary nature, each plate was characterized by using a static contact angle and a substrate material. Recording the factory default data, the first plate (referred to as Flat Plate A) had a contact angle of about $\theta \approx 88^\circ$. The second plate (Flat Plate B) had its top surface coated with a hydrophilic ($\theta < 10^\circ$) coating, and the third plate (Flat Plate C) had a hydrophobic ($\theta \approx 108^\circ$) coating. These three plates shared the same substrate material. The fourth plate (Flat Plate F) had a contact angle of $\theta \approx 110^\circ$. However, it had a different coating substrate material than the ones used in Flat Plates A, B, and C. Comparison of the data of Flat Plate F ($\theta \approx 110^\circ$) against Flat Plate C ($\theta \approx 108^\circ$) indicated frost nucleation characteristics for surfaces that shared same static contact angle but had different substrate materials and manufacturing processes.

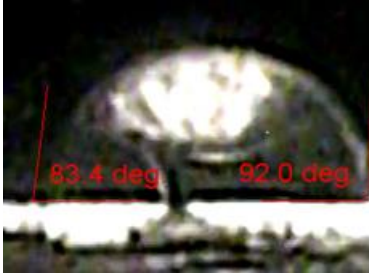

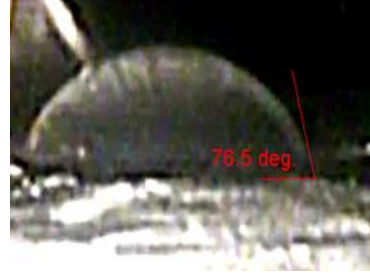
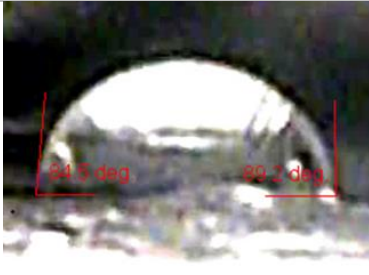

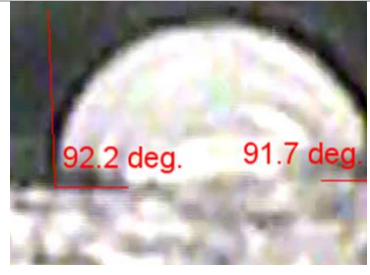
		
Test Plate A	Test Plate B	Test Plate C
		
Test Plate D	Test Plate E	Test Plate F

Figure 4.17: Contact angle measurement by using clear water droplet on different test plates.

From Figure 4.17, except for the contact angle information provided by the Circle-Proscopio, the dynamic contact angle also can be measured with the Video Scope device and Image J software. From these rough measurements, there are quite different with the factory default contact angle information. The super hydrophilic plate B and E has contact angle which is less than 10° . While from camera measured data, it shows plate B has a average 61° . The test plate E has a average number of 31.6° which is quite off with the 10° . These unclear data would provide a large amount of inconsistent experiment data. Unfortunately, there is no opportunity to do the additional measurements for investigating the surface wettability.

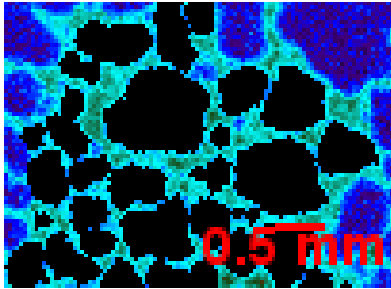
Chapter5: Discussion of the Experimental Results

5.1 water droplet size and density

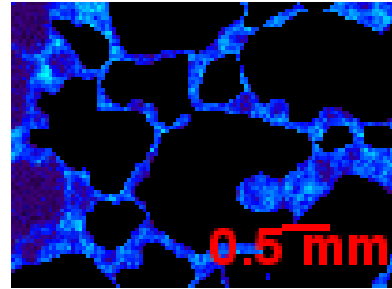
Figure 5.1 presents droplet IR images for the droplet's size and shape on each flat plate. The image for Flat Plate B ($\theta < 10^\circ$) was taken at about 7 minutes after the surface was exposed to humid airflow, while the images for Flat Plates B, C, and F were taken at about 12 to 13 minutes of continuous exposure to the air. In all cases, the surfaces were set at a temperature of 25°F. The droplets on Flat Plate B ($\theta < 10^\circ$) had the largest average diameter among all test flat plates. Because of superhydrophilic wettability properties, the droplets spread out to wet much of the test plate and had irregular shapes. Flat Plate A ($\theta \approx 88^\circ$) had a low contact angle and presented irregular droplet shapes. Flat Plate C ($\theta \approx 108^\circ$) had the same coating base with Flat Plate A ($\theta \approx 88^\circ$) but a larger contact angle. Flat Plate C ($\theta \approx 108^\circ$) showed the same irregular droplet shape as Flat Plate A ($\theta \approx 88^\circ$). But droplets on Flat Plate C ($\theta \approx 108^\circ$) were smaller and appeared more similar. On the contrary, droplets on Flat Plate A ($\theta \approx 88^\circ$) were sparser than on Flat Plate C ($\theta \approx 108^\circ$) and Flat Plate F ($\theta \approx 110^\circ$). Flat Plate F ($\theta \approx 110^\circ$) had a similar contact angle to that on Flat Plate C ($\theta \approx 108^\circ$) but a different coating substrate component. Droplets on the Flat Plate F ($\theta \approx 110^\circ$) appeared to have the same irregular shape as Flat Plate C but of larger size and a more uniform droplet size distribution.

It should be noted that the droplet sizes in Figure 6 do not necessarily have to match the average droplet diameter in Table 3. Flat Plate A ($\theta \approx 88^\circ$) and Flat Plate F ($\theta \approx 110^\circ$) had similar diameters at 12-13 minutes, while for the frozen droplet average diameter after 24 minutes, the Flat Plate F ($\theta \approx 110^\circ$) showed the largest droplets size in Table 3. It was

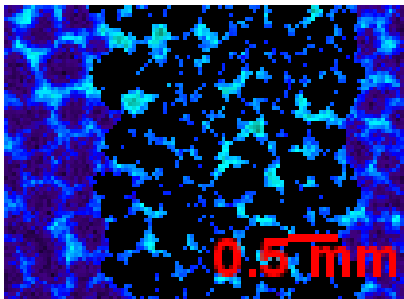
expected that larger diameter droplets would be obtained when the surface contact angle decreased (Hoke et al., 2000). However, for the flat plate types investigated in the present work and for the plate temperatures well below the freezing point as in Figure 5.1, the surface wettability effects on droplet shape were not as marked as suggested in some of the studies in the literature. In Table 3, comparing Flat Plate F ($\theta \approx 110^\circ$) and Flat Plate C ($\theta \approx 108^\circ$) under the lower surface temperature test condition, the measured average diameters were quite similar.



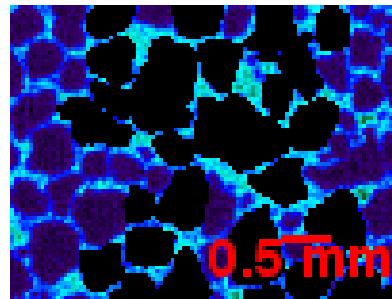
(a) Flat Plate A ($\theta \approx 88^\circ$), Average Diameter = 0.57 mm



(b) Flat Plate B ($\theta < 10^\circ$), Average Diameter = 1.19 mm



(c) Flat Plate C ($\theta \approx 108^\circ$), Average Diameter = 0.27 mm



(d) Flat Plate F ($\theta \approx 110^\circ$), Average Diameter = 0.57 mm

Figure 5.1: Average droplet diameter and droplet shape on a different flat plate with a hydrophilic and hydrophobic coating. Flat Plate B ($\theta < 10^\circ$) was taken at freezing time around 7 minutes under -3.8°C (25°F) surface temperature; images for Flat Plate A ($\theta \approx 88^\circ$), Flat Plate C ($\theta \approx 108^\circ$), and Flat Plate F ($\theta \approx 110^\circ$) with coating substrate type 2 were taken around 12-13 minutes.

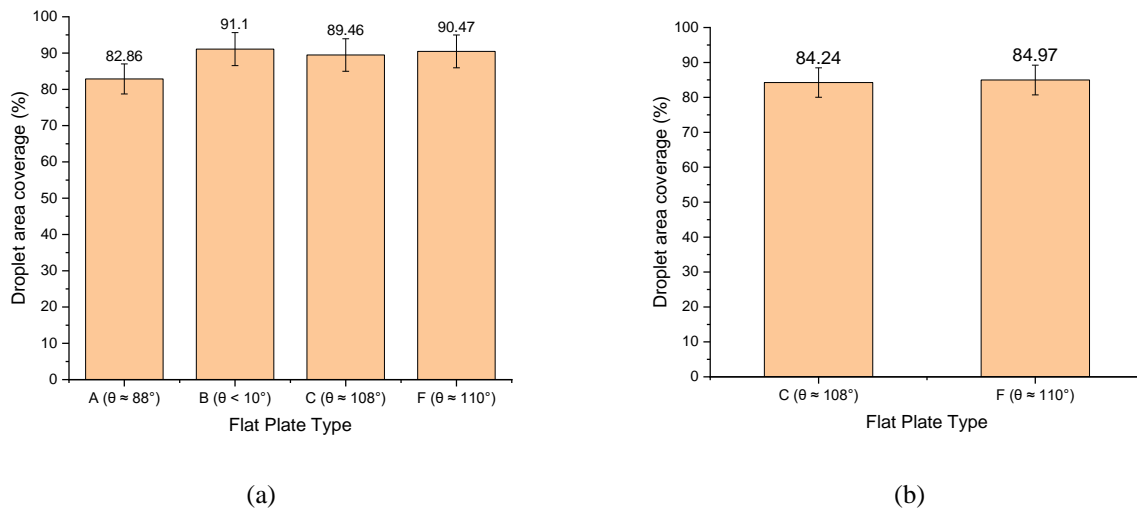


Figure 5.2: Average droplet area coverage vs different surface wettability. (a) 25°F Surface temperature test condition. (b) 23°F Surface temperature test condition.

Figure 5.2 shows the average droplet area coverage with different surface wettability and different surface temperature. As a reminder, all the droplet area coverage showed in Figure 5.2 was measured at freezing time. Flat Plate B ($\theta < 10^\circ$) had the most significant droplet area coverage than other hydrophobic test plates. Flat Plate A ($\theta \approx 88^\circ$) had the lowest droplet area coverage. From the literature study, the lower cold substrate surface temperature was expected to augment the area coverage (Sheng et al., 2020). However, Flat Plate C ($\theta \approx 108^\circ$) and Flat Plate F ($\theta \approx 110^\circ$) had the opposite trend and, as indicated in Figure 5.2, the droplet area coverage decreased by about 5% if surface temperature fell from 25 to 23°F. Because the droplets on Flat Plate C ($\theta \approx 108^\circ$) were pretty tiny at the beginning and pinned on the surface with a visible high density, when such droplets grew, the droplet area coverage increased. At 25°F, the droplets remained in the water phase for a longer time, and this more extended condensation period allowed more moisture vapor to accumulate on the cold plate. As a result, Flat Plate C ($\theta \approx 108^\circ$) and Flat Plate F ($\theta \approx 110^\circ$) had more extensive wet area coverage at their freezing time if

their surface temperature was 25°F, that is, closer (but still below) the water triple point temperature.

5.2 Measured data results and average freezing time.

Table 5.2 presents the average freezing time and average droplet diameter at the time of freezing for all flat plates and test conditions. Flat Plate B ($\theta < 10^\circ$) had the lowest freezing time. Even though Flat Plate A ($\theta \approx 88^\circ$) had a similar freezing time to Flat Plate C ($\theta \approx 108^\circ$), it still had a different average frozen droplet diameter. Flat Plate C ($\theta \approx 108^\circ$) had the lowest average droplet diameter, and the size of the droplets on Flat Plate C ($\theta \approx 108^\circ$) was pretty small. The average freezing time of all cold flat plates was dependent on surface temperature. The average diameter of Flat Plate C ($\theta \approx 108^\circ$) did not change significantly if its surface temperature decreased from 25°F to 23°F. In comparison, Flat Plate F ($\theta \approx 110^\circ$) showed that if the surface temperature dropped, the droplet sizes were measurably different. Thus, the various substrates of the coating of Flat Plate F ($\theta \approx 110^\circ$) affected droplet size and shape, but such effect was measurable when the surface temperature was equal to or above 25°F.

For the average freezing time comparison, it is obvious to see the hydrophobic surface Flat Plate A, Flat Plate C and Flat Plate F have longer freezing time comparing the hydrophilic Flat Plate B. When lowering the test plate temperature down to 23°F, the average freezing time normally decreased. In Table 5.1, Flat plate C has a slightly reduction in average freezing time when lowering the plate temperature from 25°F to 23°F. Same result to Flat Plate F, lowering the plate temperature causing the average freezing time to significantly decrease. The Plate C and Plat F have the same surface wettability under the

situation of decreasing test Plate Temperature, but the average freezing time reduction are different. That is because different coating conditions may have different water droplet sizes. The water droplet size in Flat Plate C does not change too much when it was tested on two different temperatures. Therefore, the temperature is not always dominating the water droplet or frost characteristic and freezing time results.

Table 5.1 Average Freezing time and frozen droplet diameter for each flat plates and each set of test conditions

Surface Temp.	Flat Plate A ($\theta \approx 88^\circ$)		Flat Plate B ($\theta < 10^\circ$)		Flat Plate C ($\theta \approx 108^\circ$)		Flat Plate F ($\theta \approx 110^\circ$)	
	t_s (min)	Diameter (mm)	t_s (min)	Diameter (mm)	t_s (min)	Diameter (mm)	t_s (min)	Diameter (mm)
25°F	33	1.26 ± 0.1	7	1.19 ± 0.1	29	0.98 ± 0.1	24	2.14 ± 0.1
23°F	Not Tested	Not Tested	Not Tested	Not Tested	21	0.92 ± 0.1	15	1.11 ± 0.1

5.3 Mass of Frost Accumulated on the Surfaces

In Figure 5.3, hydrophobic Flat Plate A was tested at the air temperature 41°F, and water droplet will be held as 25 °F to 26°F until becomes freezing. The constant humidity will continually provide moisture for the water/frost nucleation. The purpose for measuring the frost mass on the cold plate is to proceed calibration process. Using the high accuracy instrument to collect the water or ice on the cold plate will be complete after each experimental test. Except manually measured data, the dew point meter also automatically measured the humidity ratio from inlet to outlet of the test plate. Using $\omega_1 - \omega_2$ change to find change in water mass requires an air mass. This introduces additional uncertainty.

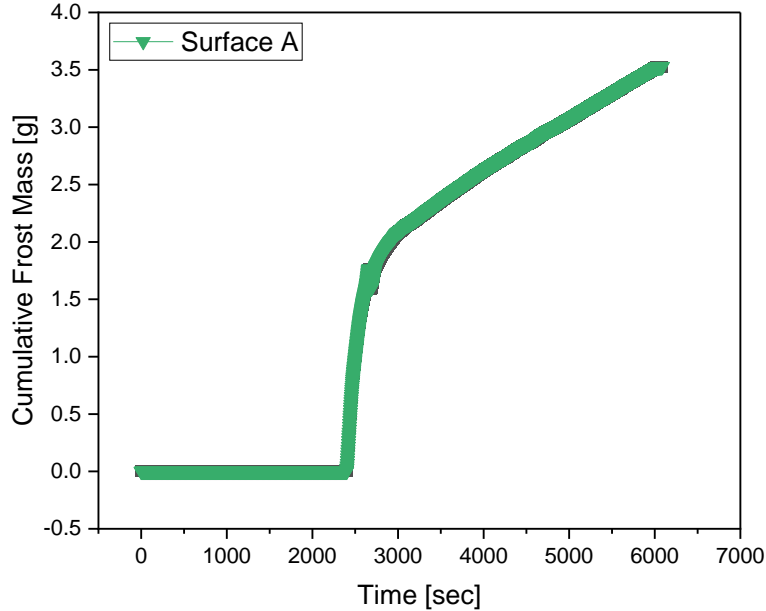


Figure 5.3: Cumulative frost mass during the experimental frosting test. *Surface A under 41F air temperature, 25 F surface temperature freezes at 3154 sec from beginning.*

5.4 Frost Thickness

Frost thickness as the main properties of frost nucleation, it can be analyzed for predicting the increasing trend and water content accumulated on the test surface. These data will play an important role in analyzing the outdoor fin type heat hump performance. For the frost growth, it can be summarized with different periods. Frost growth has two stages which are ice crystal growth and frost layer full growth. After the frost nucleation occurs, the first 20-30 minutes, the frost thickness has significant growth. It showed the porous structure and light frost density. With the moisture air continually accumulating on the frost, the top layer will have the significant frost thickness gross. It will show more condensed ice on the top layer. Then the fully frost growth period started. After starting, the frost thickness experienced a slow increase until the top frost layer reaches its maximum thickness. Different frost thickness levels have different frost shapes or structure.

No matter the porous structure or compress shape, the frost density varies with different frost structure. Therefore, the frost density has different emissivity under the infrared camera light.

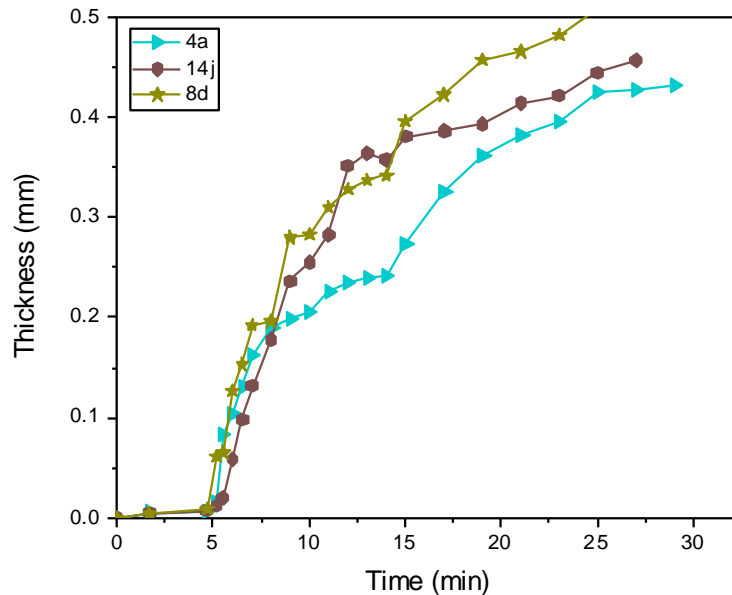


Figure 5.4: Flat Plate B: Frost thickness growth during the test period.

In Figure 5.4, super hydrophilic surface Flat Plate B was tested on different conditions. The 4a condition is the base line for this comparison. 4a is surface temperature 25°F, air face velocity 4.9 cfm. 14j condition is the same surface temperature but lower air velocity with 2.24 cfm. 8d condition is the same air velocity but lower surface temperature with 18°F. It can conclude that lower surface temperature 8d has a higher frost thickness increasing rate compared to the base line. Also, the low air velocity 14j has high frost thickness and smooth growth after the crystal frosting period. See Figure 5.4, after 15minutes, the 14j line showed a horizontal line to the end. These experiment data will be important to future predicting model in the future.

5.5 Frost Density & Frost Thermal Conductivity

The frost density is not uniform from the lowest layer thickness to highest frost thickness. With the influence of different air conditions, the earliest stage has the lowest density value, such as 50 kg/m³, while the mature frost stage has the highest density value of the ice, such as 900 kg/m³. Except the frost density varies with different structure of ice types, the frost density also depends on the position on the test plate. The front half of the test plate has denser frost than the rear area of the test plate. [Dennis O'Neal 1984] they found the average frost density on the front half of the test plate was 32% larger than the rear half of the test plate.

After frost formation, the frost thickness will experience a significant increase until frost full growth. In frost formation stage, the thickness will slowly increase. The frost density will be depended by frost structures in different periods. In crystal growth period, the frost has a porous structure and high frost density. See Figure 5.51, Super hydrophobic Flat Plate C has a increasing trend before the thickness reaches 1 mm. Normally the frost density will decrease after the liquid water freezes in solid ice, because water density is higher than frost density. Due to different surface wettability, the test plate had different freezing times. Therefore, the frost density may have different value at the same frost thickness because of different phases.

Three thermocouples were embedded inside of the frost layer with different locations. 0.5mm, 1 mm and 2mm are the thermocouples height to measure the frost layer temperature during the frost formation and growth. Except the thermocouple's measurements, the IR camera also can record the average temperature at these locations.

By adjusting the emissivity assumption of the IR camera setting, the thermocouples measured temperature and IR camera measured Temperature should be same. The collected emissivity range could be applied to calculate the thermal conductivity of different frost layers.

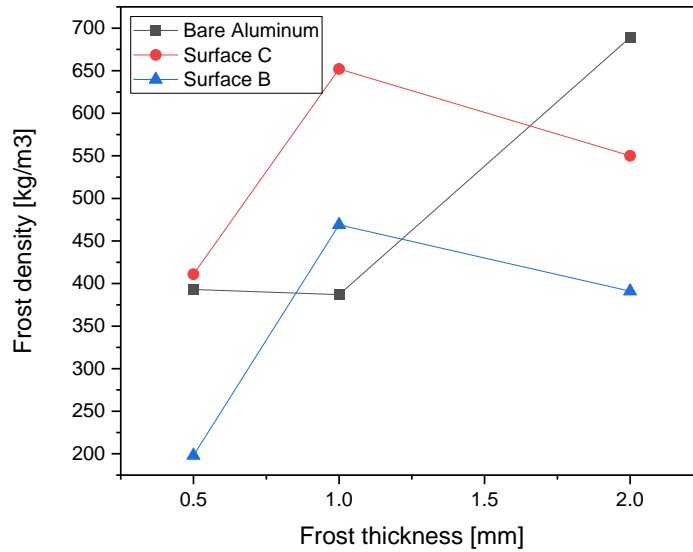


Figure 5.5: Measured frost density at three different frost layer locations.

The frost emissivity will be different and depended by frost layer thickness and frost density. Normally the emissivity of frost layer ranges from 0.8-0.95, that is shown in the IR camera. In Figure 5.6, the emissivity of frost layer decreases when frost density increases.

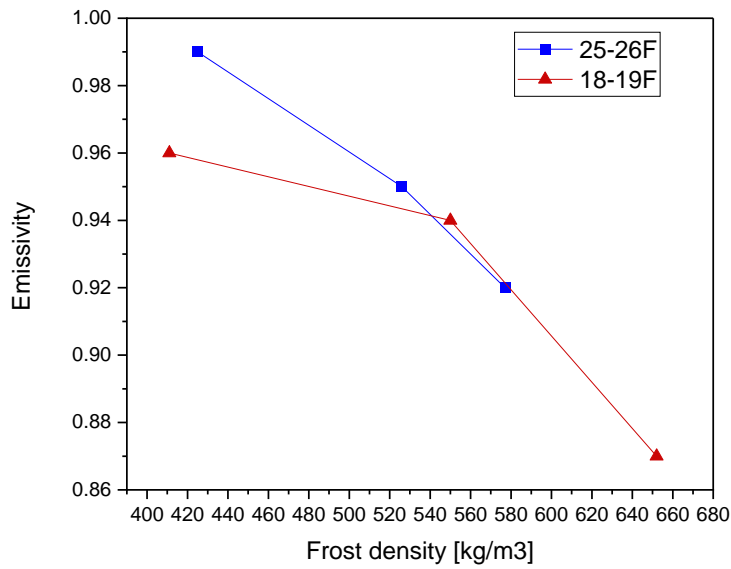


Figure 5.6: Measured emissivity corresponding different frost density.

In figure 5.7, Thermal conductivity of frost layer showed the increasing trend with the frost growth. All test plates show the same increasing trend and thermal conductivity ranges from 0.25 to 0.45 KW/M C.

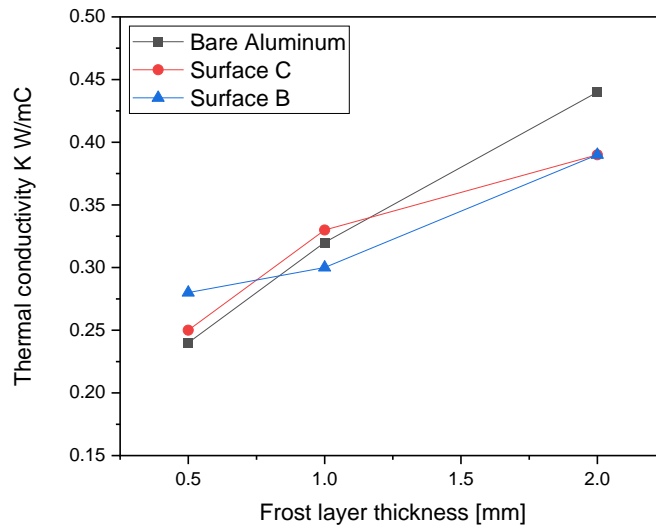


Figure 5.7: Thermal conductivity with different frost layer thickness.

5.6 Repeatability of Frost Growth Process

From the series of frost repeat test results, frost nucleation has different results. The water droplets condensed at the test plate had different shapes and phenomena. For superhydrophobic surface, the droplets started to grow from the very tiny round shape to big complete spherical shape. For superhydrophilic surface, the droplets had a very flattened and bigger shape. But for these repeat tests, the wear of surface condition, contamination particles, and different air condition parameters errors can influence the consistency of the test results.

Figure 5.8 presents freezing times for each repeated test on all flat plates at test conditions 1. Some of the repeated tests did not freeze within one hour of testing, and those tests were not included in Figure 5.61. Flat Plate B ($\theta < 10^\circ$) had the lowest average freezing time and most stable freezing time during 5 repeated tests. Flat Plate A ($\theta \approx 88^\circ$) and Flat Plate C ($\theta \approx 108^\circ$) had unstable and somewhat inconsistent freezing time within the 9 repeated tests. Flat Plate C ($\theta \approx 108^\circ$) had two trials that did not freeze within one hour; those tests were excluded from Figure 4 and were not included in the freezing time average. But the poor repeatability and large freezing times of Flat Plate A ($\theta \approx 88^\circ$) and Flat Plate C ($\theta \approx 108^\circ$) are still reported in this figure to clearly show the contrast to the data of Flat Plate B ($\theta < 10^\circ$). The first repeat test of Flat Plate C ($\theta \approx 108^\circ$) was excluded because its freezing time was over 1 hour, while the third repeat test of Flat Plate C ($\theta \approx 108^\circ$) had a freezing time of around 13 minutes only. These inconsistent freezing results might be caused by high test surface temperature had low dependence on surface wettability.

As a reminder, Flat Plate F ($\theta \approx 110^\circ$) had a very close contact angle to Flat Plate C ($\theta \approx 108^\circ$), but Flat Plate F ($\theta \approx 110^\circ$) had a different coating substrate. Unlike Flat Plate A ($\theta \approx 88^\circ$) and Flat Plate C ($\theta \approx 108^\circ$), there was only one test on Flat Plate F ($\theta \approx 110^\circ$) which froze within one hour of testing. All other repeated tests on Flat Plate F ($\theta \approx 110^\circ$) were unfreezing within two-hour test periods. Thus, it was challenging to compare Flat Plate F ($\theta \approx 110^\circ$) with other test plates in Figure 5.61 with respect to freezing time. Analysis of the average droplet size at the same test run time was still possible for all tested flat plates. The details of the droplets IR images will be shown and discussed in the next section.

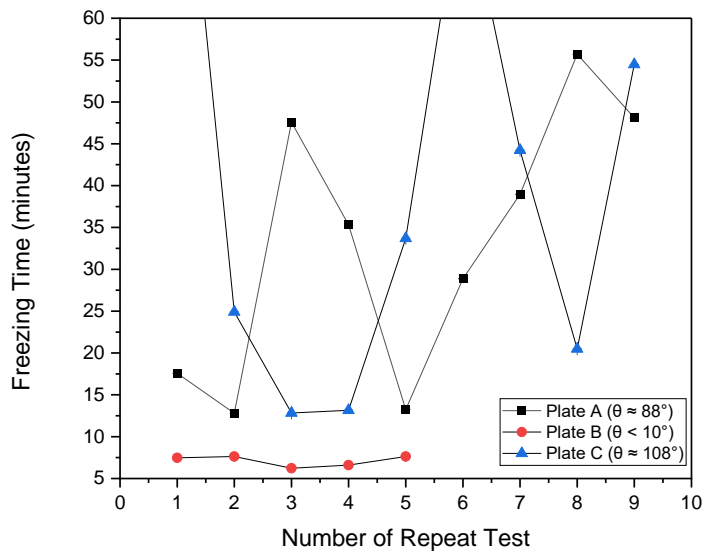


Figure 5.8: Freezing time vs. number of repeat tests for Flat Plate A ($\theta \approx 88^\circ$), Flat Plate B ($\theta < 10^\circ$) and Flat Plate C ($\theta \approx 108^\circ$) under test conditions 1. ($T_s = 25^\circ\text{F}$, $T_{a,in} = 41^\circ\text{F}$, $\omega_{in} = 80\% \text{ R.H.}$, $V_a = 3.8 \text{ m/s}$)

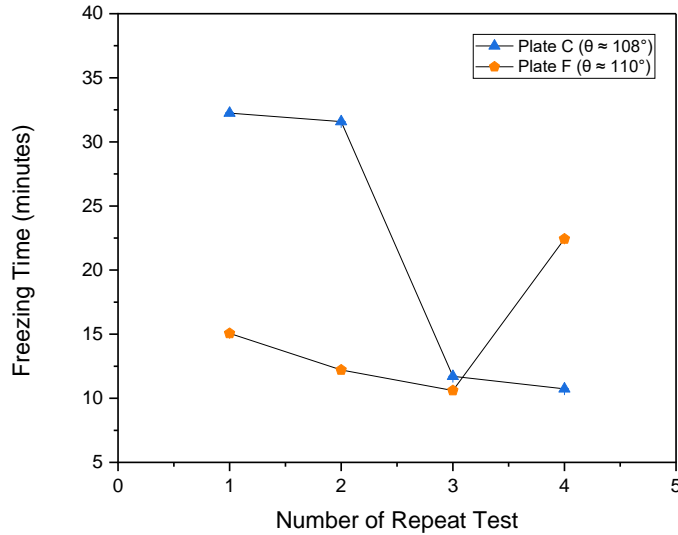


Figure 5.9: Freezing time vs. number of repeat tests for Flat Plate C ($\theta \approx 108^\circ$) with coating substrate type 1 and Flat Plate F ($\theta \approx 110^\circ$) with coating substrate type 2 under test conditions 2. ($T_s = 23^\circ\text{F}$, $T_{a,in} = 41^\circ\text{F}$, $\omega_{in} = 80\%$ R. H., $V_a = 3.8$ m/s)

Figure 5.9 presents freezing times for Flat Plates C ($\theta \approx 108^\circ$) and F at test conditions 2. For test conditions 2, the surface temperature was reduced to 23°F , and four repeated tests were performed for the different flat plates. Compared to Flat Plate C ($\theta \approx 108^\circ$), Flat Plate F ($\theta \approx 110^\circ$) had less variability of the freezing time and, in average, it had a shorter freezing time. That shows that the surface wettability of Flat Plate F ($\theta \approx 110^\circ$) had a significant effect on freezing time in this series of repeat tests.

From a literature review study, researchers (Kim et al. 2016, Zhang et al. 2016, Wang et al. 2014.) pointed out that surface wettability can delay the freezing time. Harges et al. (2020) showed that when relatively high sub-freezing plate temperatures were used, the test plates' surface wettability had a minor impact on the freezing time. The authors' previous work also highlighted that minor surface imperfections could inhibit the surface wettability effect and delay freezing. When comparing two different surface temperature

test conditions, it was observed that Flat Plate C ($\theta \approx 108^\circ$) had a more stable freezing time region when its surface temperature was 23°F. Flat Plate C ($\theta \approx 108^\circ$) had inconsistent freezing times at the higher surface temperature, and the root causes of this behavior are unclear and require further investigation. In particular, analysis of this surface before and after multiple frost and defrost processes could shed some light on potential surface modifications and contamination affecting the freezing time during the run time at 25°F.

The average freezing times for the cold flat plates investigated in the present paper depended on their surface temperatures. Superhydrophilic Flat Plate B ($\theta < 10^\circ$) had the shortest freezing time, and it ranged between 6 and 7 minutes. Flat Plate A ($\theta \approx 88^\circ$) and Flat Plate C ($\theta \approx 108^\circ$) had longer freezing times than the superhydrophilic coated Flat Plate B. Repeated tests of Flat Plate A ($\theta \approx 88^\circ$), C ($\theta \approx 108^\circ$) showed that freezing time had large fluctuations, ranging from 13 up to 56 minutes. However, if surface temperature decreased by only a few degrees, then a much narrower span of freezing times was observed.

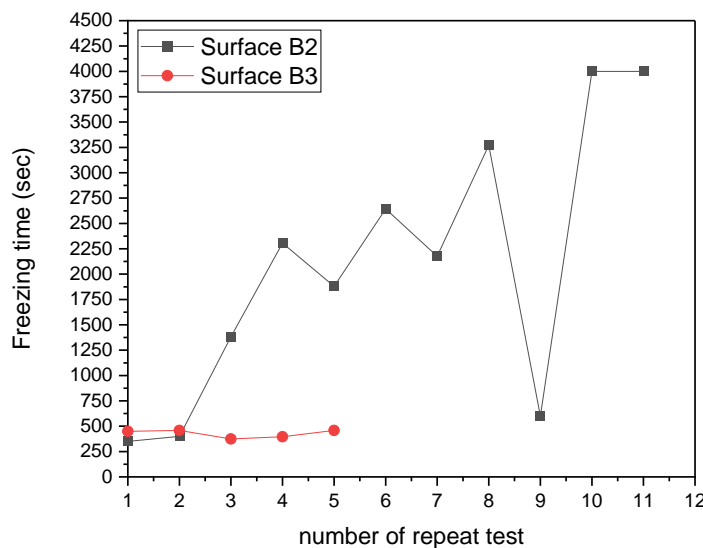


Figure 5.10: each freezing time at different repeat test.

The two same surface wettability plates were tested in this comparison. See Figure 5.10. With the same test condition, Flat Plate B2 and B3 showed different freezing results. In the first two repeat test day, it has the same freezing time. Starting from the third repeat test, surface B3 still has stable freezing time results. While the Surface B2 has inconsistent freezing time results. This may be caused by different cleaning methods, chemical coating destroyed with the number of repeat test increasing and contamination particles effect.

5.7 Summary of the findings and lesson learnt from Experimental Work

The IR images of the present work showed that the static contact angle of the surface had a weak effect on the shape of the droplets before they turned into iced beads. For a similar contact angle of $\theta \approx 108^\circ$ to 110° , the substrate had a measurable effect on the droplet diameter when the surface temperature was at least 25°F or above. Hydrophobic surfaces investigated in the present work showed somewhat irregular splattered droplet shapes. This intriguing visual observation from the IR images appeared not consistent with the data shown in some literature studies (for example, in Harges et al. 2020). It might be due to differences in the specific surface coating chemistry and substrate materials of the flat plate investigated in the present work. Further investigations should be conducted in future research before comparing the droplet shapes from surfaces with similar static contact angles with different chemistry of the coatings.

Chapter 6-- Development of the Analytical model

6.1 Thermodynamic and Heat Transfer model

When moist air was cooled, water vapor from the air steadily condensed on the cold plate if the cold plate temperature is below the dew point temperature of the incoming air stream. The water vapor, liquid water and solid ice can coexist at triple points, lowering the temperature or increasing the pressure could speed up the freezing process of water at a temperature below 0°C. At the variable environment condition, the water droplet may have different freezing result. Starting with the Classical nucleation theory (CNT), it is important to note that the ice nucleation is sensitive to the impurities in one single droplet. Higher nucleation rate controls the system to be freezing earlier. A lower nucleation rate delayed the ice crystals appearing even at lower temperatures. Due to different impurities of the system, homogeneous nucleation seldom occurs in the natural environment because of its nucleation sites should be suspended in the air and away from the surface. Instead, heterogeneous nucleation occurs frequently on the surface as the nucleation sites. Starting from a metastability state, water molecules leave from the resting state and transfer to a higher energy state. Macromolecules or clusters spontaneously change to the thermodynamic equilibrium state.

From the inconsistent experimental freezing time results, looking at the internal structure of one single water droplets could explain the random freezing phenomenon. In order to illustrate how the contamination particles affect the single water droplet to accelerate the freezing process, a model of one single water droplet is necessary to be provided.

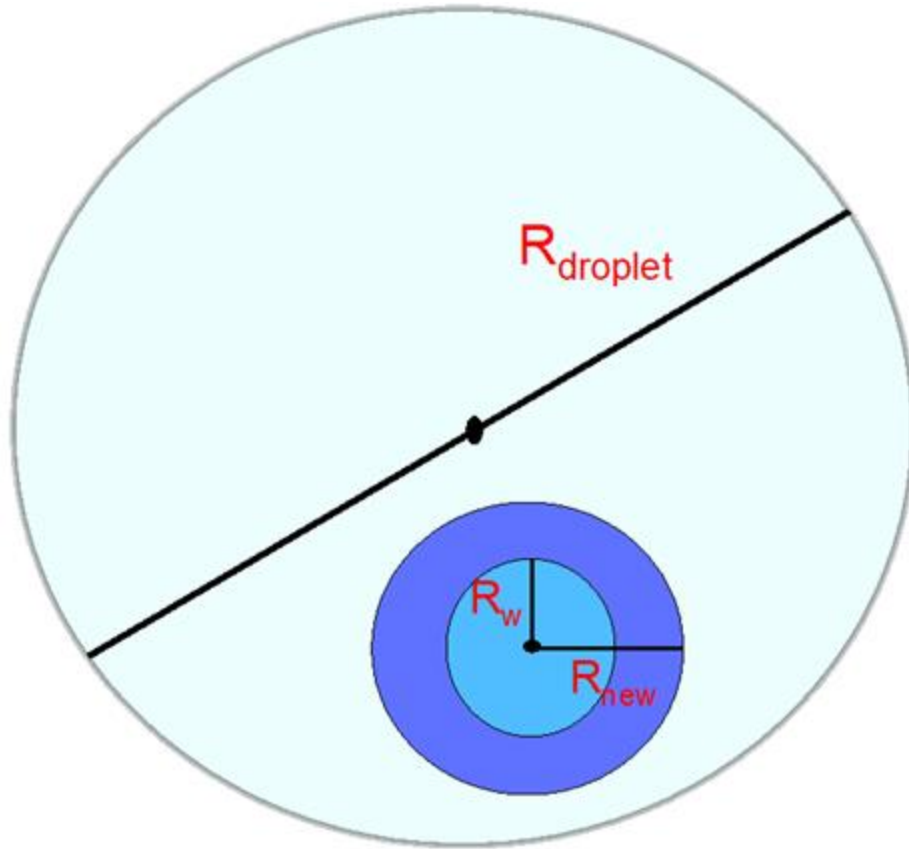


Figure 6.1: Schematic of the Pure Water Droplets to describe the modeling work of Nucleation Theory.

In Figure 6.1, Within one single water droplet, there are several molecules and other items include the water molecules, ice embryos, and contamination particles. The ice embryo could be act as the seeds of causing the whole water droplets frozen and its radius is R_w . The contamination particles come from the air pollution and top surface of the test substrate stayed inside of the water droplet. The contamination particles vary from different size and could be acted as the main reactants to enlarge the original ice embryo size to become a larger new cluster. The new ice cluster has a radius R_{new} which could be assumed as the combination of the original water molecules cluster

$R_{w-no\ contamination}$ and contamination particles. For a simple description, the $R_{cluster,ice\ embryo+contamination\ particle}$ can be write in R_{new} , while the water molecules cluster or ice embryo cluster could be write in the $R_{w-no\ contamination}$. When the contamination particles have a reaction with the water molecules or ice embryo clusters, it not only enlarges the size of the ice cluster, but also accelerates the speed of the freezing.

A concept for describing the relation between the contamination particles size and pure single water droplet would be shown. The Contamination factor (Cf) is a number that describes the scale of the combined cluster compared to the scale of the ice embryo with no contamination. The definition of contamination factor Cf is as follows:

$$C_f = \frac{R_{cluster,ice\ embryo+contamination\ particle}}{R_{w-no\ contamination}} \quad (6.1)$$

Considering the indoor environment, the assumption of contamination particles is provided for the next calculation. The combined Cf factor ranged between 1 and 3000 so that

$$R_{w-no\ contamination} \leq R_{cluster,ice\ embryo+contamination\ particle} \leq R_{water,droplet}$$

The Cf factor varies from the different scale, defining the contamination particles as a detectable range by the inside visual inspection of wind duct. The example for Cf factor calculation and assumptions were shown in next section. With the contamination level increased, more and more ice embryo clusters grew up faster by combining the contamination particles. To explain the theory of contamination particles accelerated the ice embryo freezing process, the Classic Nucleation Theory (CNT) could be introduced.

The total free Gibbs energy of the system changed defined with ΔG . The $\Delta G = 0$ is necessary for equilibrium condition of the system. Controlling the surroundings, the Gibbs free energy (G) is introduced to explain the minimum thermodynamic equilibrium in closed system at constant temperature and pressure. $G = U - TS + pV$. Chemical potentials for each component will be constant and chemical potential of water molecules can be defined from the differential equation $dG = -SdT + Vdp$. Suppose that the ice cluster has a number i of molecules. If the number of i molecules increased, the size of ice cluster would increase. In the formation of ice cluster, the total free energy of the system is changed by

$$\Delta G = \Delta\mu i + Ai^{\frac{2}{3}} \cdot \mu \quad (6.2)$$

μ is the chemical potential of molecules in the liquid system. The equation above can be applied to ice clusters for all sizes. When a critical size i^* is reached, the rest molecules and ice-like cluster can quickly freeze into macroscopic crystal. The maximum value of ΔG is ΔG^* which gives the top of the thermodynamic nucleation barrier. If we make the assumptions, the ice embryo formation in the liquid water droplet will obey the classical nucleation rules and shows the stationary distribution for generating the nucleation rate J . The concept of the ice nucleation rate J could be used to predict the freezing time. From the ice embryo growth phase, the size of ice-like clusters reaches the critical radius r^* could cause a time delay. The delay freezing time depends on the ice nucleation rate J and critical size r^* of the ice embryo before completely frozen.

The impurities in the air and contamination particles adhered at the groove of test substrate have different micro-level both can affect the nucleation rate. Illustrating all assumptions and introducing the combine Cf factor is necessary before entering the next section.

For the pure water cluster case, there are several assumptions for calculating the Cf factor. Firstly, Iced molecules freeze and occupies the rest of the space of the whole water droplet. Secondly, there is not an actual chemical reaction between substrate and water/ice molecules but the merging of a water molecule into an embryo resemble a chemical process and it can be described by similar chemical reaction rules. Thirdly, The smallest water cluster size can be assumed as 75 nm at the temperature -40°C , which means radius of single water clusters (contain 275 normal water molecules) is 75 nm. For the contamination particles within the water droplet case, there are also other different assumptions that could be needed to illustrate. The size of contamination particles suspended in the air can vary from 0.27 nm to 2500 nm based on the lab wind tunnel air filter information about dust size less than PM 2.5 (0.25 microns μm). The water cluster and contamination particles are both spherical shape in this model and the new water molecules cluster group combined with contamination particles are also treated as simple sphere shape. Finally, Surface tension between the new cluster and ice embryo is constant at specific temperatures. Surface tension σ may reduce 30-40% by inserting the contamination particles. Surface tension σ does not change with the size of ice embryos. Some other assumptions and parameters for the calculation are presented in the Appendix.

6.2 The calculation of Free Gibbs energy with different ice embryo size under variable Cf factor.

This model was used to predict the actual freezing time of a single water droplet on the test substrate. Except for adding the new concept of contamination factor, the actual freezing time still could be obtained from the Classic Nucleation Theory (CNT). In order

to understanding the model details and novelty part, an example of showing calculation is necessary to be provided.

Next is an example of Surface A at the surface temperature 25 °F that calculate the predicted time t_f in next several steps.

Step1: Input from the experiment data:

Surface Temperature	25 °F
Contact angle	87.25°
Air temperature	42 °F

Step2: Input parameters:

Surface tension σ	16; (unit: erg cm ⁻²)
R_w	0.2 (unit: nm)
Nucleation rate	9.1700e+07 (unit: cm ⁻³ s ⁻¹)

Illustration: surface tension is a constant assumption. Normally the average surface tension between water liquid surface to solid phase surface is 26-28. Because of considering the contamination particles effect on the pure water freezing process, the surface tension σ had a 10-30% reduction. Surface tension 16-18 could be taken in the model calculation.

R_w is assumed constant based on the lowest water molecules cluster size.

Nucleation rate is assumed by applying the equation of $J \sim 10^{27} \exp(-\Delta G^* / kT)$. Where the k and T depends on the supercooled temperature range of water droplets. Nucleation rate is

constant for each test plate and surface temperature. It is relevant with contamination particles levels.

Step 3: Main Calculation loop in this model.

The critical radius calculated from the equation shown below,

$$\Delta G(r) = \frac{4}{3}\pi r^3 \Delta G_v + 4\pi r^2 \sigma \quad (6.3)$$

Equation 6.3 has two terms, the left term ΔG_v related the chemical potential μ between ice and water, while the right term depends upon the shape of the cluster and the structure of the interface. This equation was taken from Webb's model, the interface is characterized by a surface free energy σ . Therefore, ΔG_v could be calculated and its procedure shown as below, the surface tension σ can be assumed constant as 16 (erg/cm²) from the input Step 2 table.

Still stay in Step3, in equation 6.3, Before plotting the correlation between ΔG and radius r of the ice embryo during the whole freezing process, it is necessary to calculate the parameter free energy difference per unit volume between ice and water ΔG_v

Recall the thermodynamic relation $S = - \int_0^{\Delta T} \Delta S_v d\Delta T = -\Delta S_v \Delta T$, where the ΔS_v is an average entropy of fusion over the supercooling range. Recording the experimental setup, the ΔT could be applied as 40 °C. In Webb's model, a simple approximate value for water has been applied, the equation becomes:

$$\Delta S_v \approx (1.13 - 0.004 \Delta T) \times 10^7 \text{ erg cm}^{-3} \text{ deg}^{-1} \quad (6.4)$$

After having the ΔS_v and surface tension σ , using equation (6.3) which is $\Delta G(r) =$

$\frac{4}{3}\pi r^3 \Delta G_v + 4\pi r^2 \sigma$ could calculate the total free energy of the system is changed by a amount.

Where $r = R_{cluster,ice\ embryo+contamination\ particle}$.

Notice that the r in equation 6.3 had its own path in modeling, which varied from the smallest size as the pure water molecules to a large water clusters size. When the ice embryo continues growing within the water droplet, the size might reach the critical radius of the ice embryo which has the highest free energy of the system. Because the water molecules reached the critical radius, the energy hit the maximum barrier to cause the phase change from liquid to solid ice. Also calculating the size of the critical embryo in the nucleation process would explain ice-like clusters of near-critical size exist in the physical situation.

Step 4: Plot the total free Gibbs energy of the system changed vs radius of the ice embryo clusters.

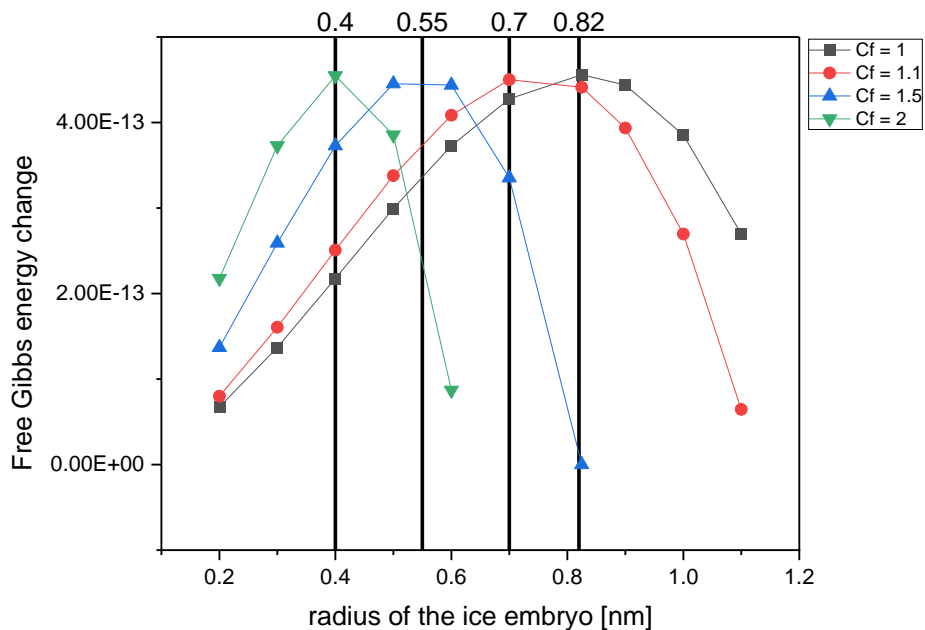


Figure 6.2: Free Gibbs energy changes with the radius of the water/ice cluster under different contamination levels.

With adding the contamination particles, the calculated critical radius for free Gibbs energy is getting smaller. The results are shown in Figure 6.2.

ΔG^* gives the height of the thermodynamic barrier to nucleation or freezes at the particular temperature. From the figure, each maximum Gibbs energy has its own critical radius to stand for freezing into crystal structure from liquid phase. The critical radius of free Gibbs energy when C_f equal to 1 shows 0.82 nm in Figure 6.2. Ice embryos started from its original size to grow up to 0.82 nm, 0.82 nm ice embryo contains enough energy for ice nucleation and freezing into ice crystal. With the contamination level increased from $C_f = 1$ to $C_f = 2$, the critical radius reduced from 0.82 nm to 0.4 nm. For ice embryo size nucleation process, some ice embryos may reach the critical size earlier by inserting the contamination particles. Because inserting contamination particles could enlarge the original critical size of the ice embryos group. When the radius of ice embryo is very small, small ice clusters are unstable and tend to disappear and rather grow. When $C_f = 1$, there are no contamination parties affect the pure water droplet. With the C_f change from 1 to 2, the unstable region like 0.2 nm to 0.8 nm will become short. With the contamination factor C_f increased, the critical radius of the ice embryo occurs earlier than if there is no contamination case.

Table 6.1 Example of the model intermediate values and resulting freezing time:

	Surface A	Surface B	Surface C
Input	Input	Input	Input
T_surfacers	25°F(3.8°C)	25°F(3.8°C)	25°F(3.8°C)
Contact angle	87.85°	<10°	107.75°
T_air	41°F (5°C)	41°F (5°C)	41°F (5°C)
Surface tension σ	22 (erg/cm ²)	22 (erg/cm ²)	22 (erg/cm ²)
C_f	16.6	29.76	11.73
F	1e+12	1e+12	1e+12
Intermediate Values			
ΔG at the critical radius	4.56E-13	4.46E-13	4.46E-13
Rc	0.05 (cm)	0.03 (cm)	0.07 (cm)
Output	Surface A	Surface B	Surface C
Freezing time sec	1031 seconds	688 seconds	1238 seconds

6.3 Contact angle function model with different Cf levels

Except impurities suspended in the air effect on the onset nucleation or freezing, the surface wettability also can affect the free Gibbs energy change. If considering the contact angle pitch or roughness of the test plate, the heterogeneous model will be modified based on the homogeneous nucleation.

The critical free Gibbs energy of heterogeneous will be

$$\Delta G_H^* = \Delta G^* f(m, R) \quad (6.5)$$

Where the $f(m, R)$ function will be calculated from the equations: $f(m, R) = \frac{1}{2}(m, x, h)$

Where $h = (1 + x^2 - 2mx)^{1/2}$, $x = R/r^*$ and $m = \cos(\theta)$.

Contact angle θ varies from $0 - 180^\circ$ in this model. The results show in Figure 6.3,

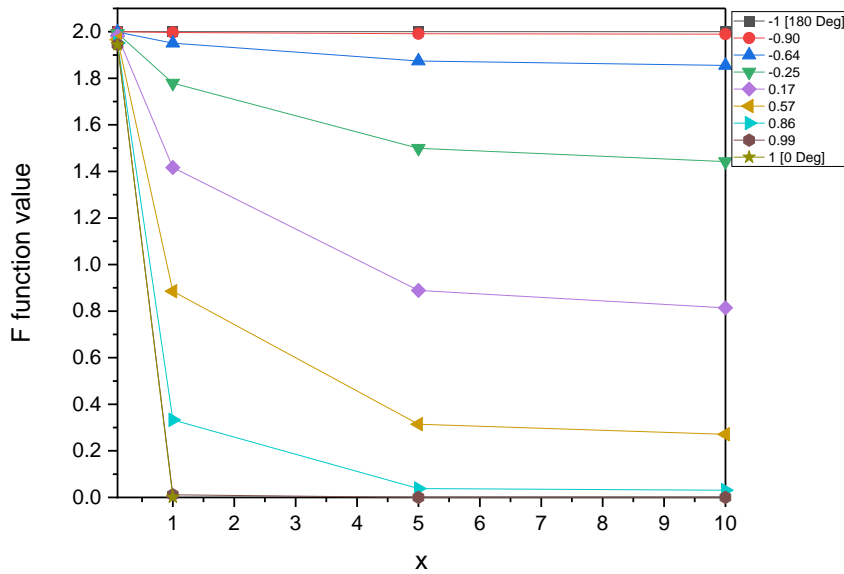


Figure 6.3 F function with x for transferring heterogeneous model.

In Figure 6.3, the F function value decreased from 2 to 0 when contact angle varies from 180 to 0. Super hydrophobic has high F function value and high free Gibbs energy.

The hydrophobic surface is closer to heterogeneous nucleation and has short freezing time. And super hydrophilic surface has lower Gibbs energy and is close to homogenous model.

Another comment to this result, the Contamination factor Cf is increasing, make the hydrophobic surface (130°) wettability close to the hydrophilic surface (55); Cf changed the surface wettability and make it freeze easier.

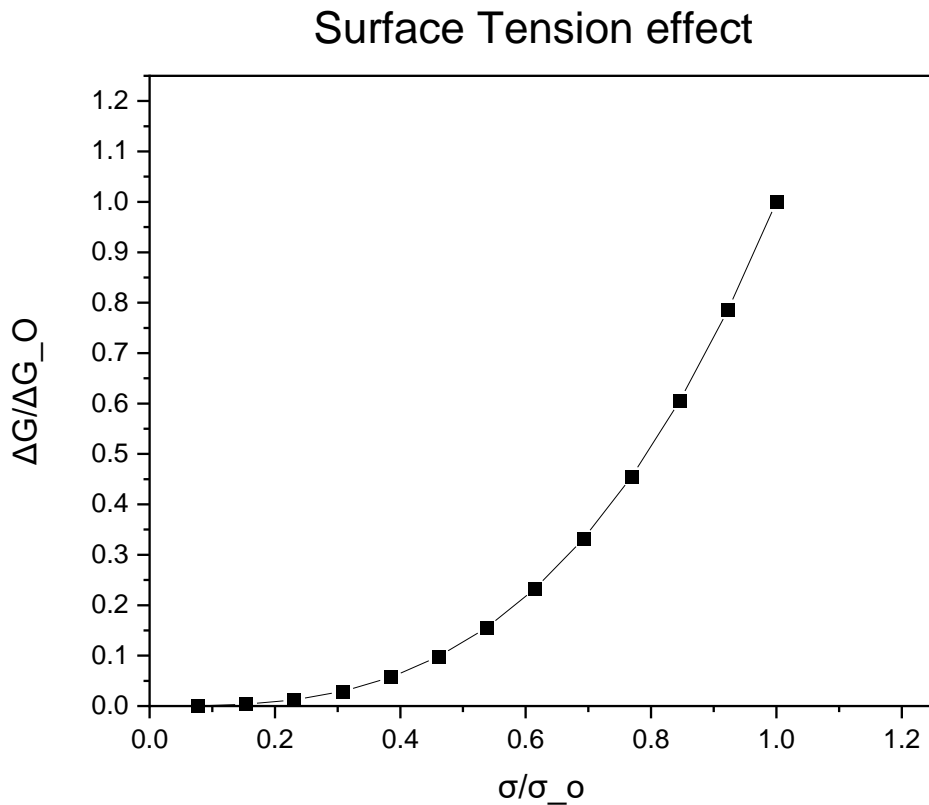


Figure 6.4: surface tension reducing effect for free energy change.

Without the contamination, the sigma (surface tension) = 26, decreasing sigma from 26 to 1, see the ratio of sigma_c/sigma change, plot the gibbs energy and critical radius change with the sigma.

When the ratio of sigma equals to 1 means there is no surface tension reduction due to purify surface condition and air quality. $26/26=1$ for σ (surface tension) from the

literature data. With the assumption going, the test plate surface condition is getting certain amount of dust particles and with the same air quality issue, the ratio of σ is reducing to left from 1-0.2. The product result we should observe the ΔG ratio change.

σ_o (surface tension between ice embryo to solid plate) is the purify case; ΔG_o (critical gibbs energy change) is the purify case.

6.4 Combine Cf factor from air contamination and substrate surface contamination.

Normal Contamination particles suspended in the air have the size range and most of them are filtered by air filter in the wind tunnel. The maximum value depends on the PM 2.5. Except for the air contamination effects, the contamination particles on the top surface of the test plate could change the certain surface wettability. Combining the air contamination and surface contamination particles is necessary for investigating the free Gibbs energy. Which side contamination dominant the critical radius and ice nucleation rate needs to be answered in this model.

The δ is calculated from the equations below: $\delta = \frac{A}{A_{tot}}$, where the spherical cap area calculation equations are:

$$\text{Cap height: } h = \sqrt{r^2 - a^2} \quad (6.6)$$

$$\text{Cap radius: } a = \sqrt{r^2 - (r - h)^2} \quad (6.7)$$

$$\text{Cap surface area } S = 2 \cdot \pi \cdot r \cdot h \quad (6.8)$$

$$\text{Cap base area } A = a^2 \cdot \pi \quad (6.9)$$

Contact angle can be used for this calculation to decide which portion of the area is dominant. For example, δ depends on the Surface contact angle Θ . When the $\Theta = 90$, The

$\delta = \frac{A}{A_{tot}} = 0.5$, When $\Theta = 180$, $\delta = \frac{A}{A_{tot}} = 1$, there will be very small portion of the water droplet sit on the test top surface.

Therefore, the combine Cf equation is: $Cf = [\delta \times Cf_{air}] + [(1 - \delta) \times Cf_{surface}]$; $0 < \delta < 1$.

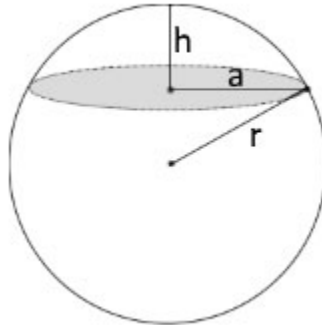


Figure 6.5: Schematic for calculating the area ratio δ .

The calculated combine Cf factor will be reentered into the Free Gibbs energy calculation loop to find the new critical radius for predicting freezing time.

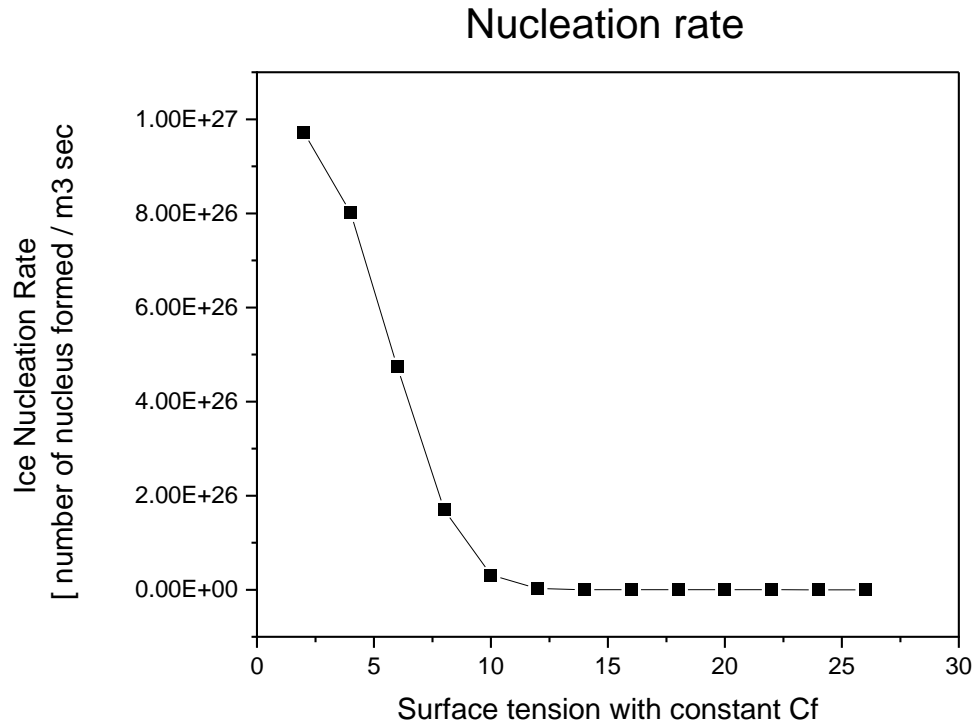


Figure 6.6: surface tension effect on ice nucleation rate.

From the figure 6.6, we can see when the surface tension reduced from 26 (purify plate) to 1, the ice embryo nucleation rate increased significantly, especially sigma starting from 10 to 1. From the literature data, the authors pointed out with the certain amount contamination, the surface tension can have 20-30% reduction. Sigma from 26 to 10, the nucleation rate still changes a lot but slowly comparing 10 to 1.

6.5 Predicted freezing time from calculated nucleation rate.

The predicted freezing time acts as the main frost characteristic and is usually used for analyzing the surface wettability and air condition variables. The frost nucleation rate is defined as numbers of nucleus formed per unit volume in unit time. The water droplet or ice embryo groups are assumed as a spherical structure. Thus, with certain assumptions,

frost nucleation rate could be applied for calculating the predicted freezing time for frost nucleation.

The main correlation for calculating the predicted freezing time is:

$$tf = \left(\frac{r_c - r_0}{I_c} \right) \times F \quad (6.10)$$

Where the r_0 is the original water molecule radius. r_c is the ice embryo critical radius. I_c is the current temperature nucleation rate. F is a constant value calculated from minimizing the errors between the predicted freezing time and the experimental data. It should be noted that the experimental data of the present work were predicted by using one constant F for each flat plate surface temperature. At 25°F, the value of F was 1e+12 while at 23°F the value of F was same as the value of 1e+12. That because 2°F drop of subcooled temperature especial when it occurs at the temperature closer to the water freezing point 0°C won't affect the ice nucleation rate I_c too much. Thus, the constant adjusted factor F could be still assumed same at both temperature of 25°F and 23°F. However, when subcooled temperature range is extremely low, such as 30°C or 40°C, the ice nucleation rate would have a significant change. In order to prove this scenario, additional discussion was provided with figure 6.43. In figure 6.43, the decreasing the surface temperature would have a large subcooled temperature range. Starting at the subcooled temp at 20°C (surface temperature -4 °F), the ice nucleation has a significant increasing. At lower surface temperature the constant adjusted factor F in this model would assume much larger (such as 1e+16) to have a stable predicted freezing time.

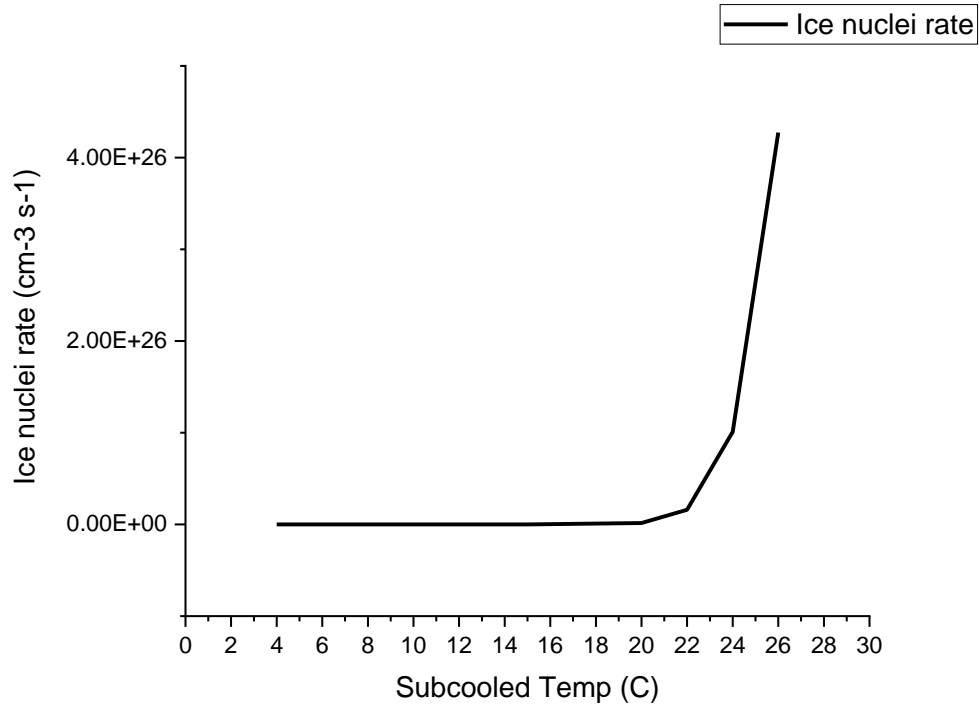


Figure 6.7: The ice nucleation rate changes with the different subcooled water droplet temperature.

For the same surface and same testing conditions, the variability of the freezing time from one test to the other was supported by a possible variation of the level of particles contamination of the surface. Such contamination was the result of air quality, water droplets residuals from previous freezing cycles, and cleaning of the surface prior to the test. The level of contamination was lumped into one parameter, defined as C_f , which varied from 11 to 31.

For each surface wettability, submit the C_f factor to model and get the new critical radius. Because when ice embryo reached the critical size, freezing process was assumed to be occurred. From the nucleation rate calculation, 25 F° and 23 F° will have different constant nucleation rate. Although many researchers predicted the actual freezing time by

using the water formation rate of ice nucleation rate, inserting contamination factor combined with the contact angle would be considered in this model. From figure 6.7, the nucleation rate does not have too much change when surface tension decreased from 26 to 10, therefore surface tension 22 will be applied in the freezing time prediction. By varying the surface tension from 26 to 20, there are still many different predicted results in this model.

Except the contamination factor and contact angle structure, the chemical coatings and surface roughness are not considered. For example, test plate B and test plate E both has contact angle $< 10^\circ$; test plate A and test plate D both has contact angle around 88° ; but the prediction shows the same combine Cf level for the same contact angle surface, that means the prediction results could be same for the same contact angle without considering chemical coatings. These limitations also will be discussed in the relevant scenario's sections.

Chapter7--Model results and comparison with the data

7.1 Comparison of modeling results with data of the current work

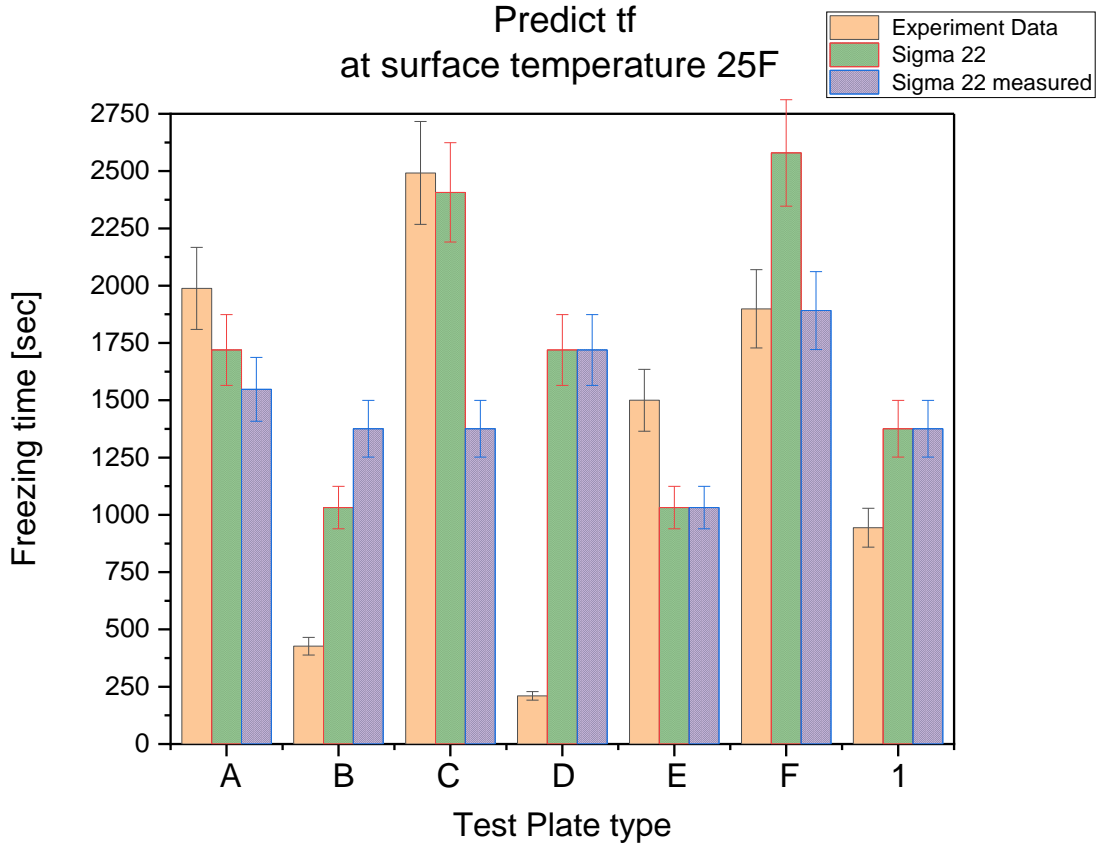


Figure 7.1: Predict freezing time of different surface wettability comparing the experiment test data at plate temperature 25 F (constant $F = 1e+12$).

The error bar of experiment data is 25%. The sigma22 is the predict model result and its error bar depends on the nucleation rate 25% variable. The sigma22measured is a prediction model with same assumptions except using the measured contact angle, it should be closer to experiment data theoretically. Test plate 1 is bare aluminum surface which can be treated as the base line for comparisons. Surface tension 22 was assumed constant for calculating the predicted freezing time. In figure 7.1, at the surface temperature 25 F the

bare aluminum plate has a average freezing time of 970 seconds. The predicted freezing time is very close to the base line. Varying the surface tension from 26 to 22, the corresponding nucleation rate is different. Choosing the suitable nucleation rate can easily calculate the predicted freezing time. For the same contact angle 110° comparison, test plate C and test plate F both have the longer freezing time. No matter using the measured contact angle or factory contact angle, it can predict the freezing time and is in line with the actual experimental data. For super hydrophilic surface, the combine Cf model has large Cf value. Because large Cf combine value means there are large portion of one water droplets attached on the top surface of the test plate. The contamination particles sticking on the grooves of the pitch spacing of the contact angle could change the surface wettability. Thus, large Cf combine will lead to small critical radius for ice nucleation. The predicted results will meet the lowest freezing time phenomenon of low contact angle surface experiment data. Although most test plate freezing times were well predicted, there are still two plates out of the prediction results in this model. Unfortunately, test plate D and test plate E do not have too many repeat tests. Due to uncertainty of the experiment and inconsistent contamination particles, the prediction of test plate D and test plate E would not conform to the actual single result.

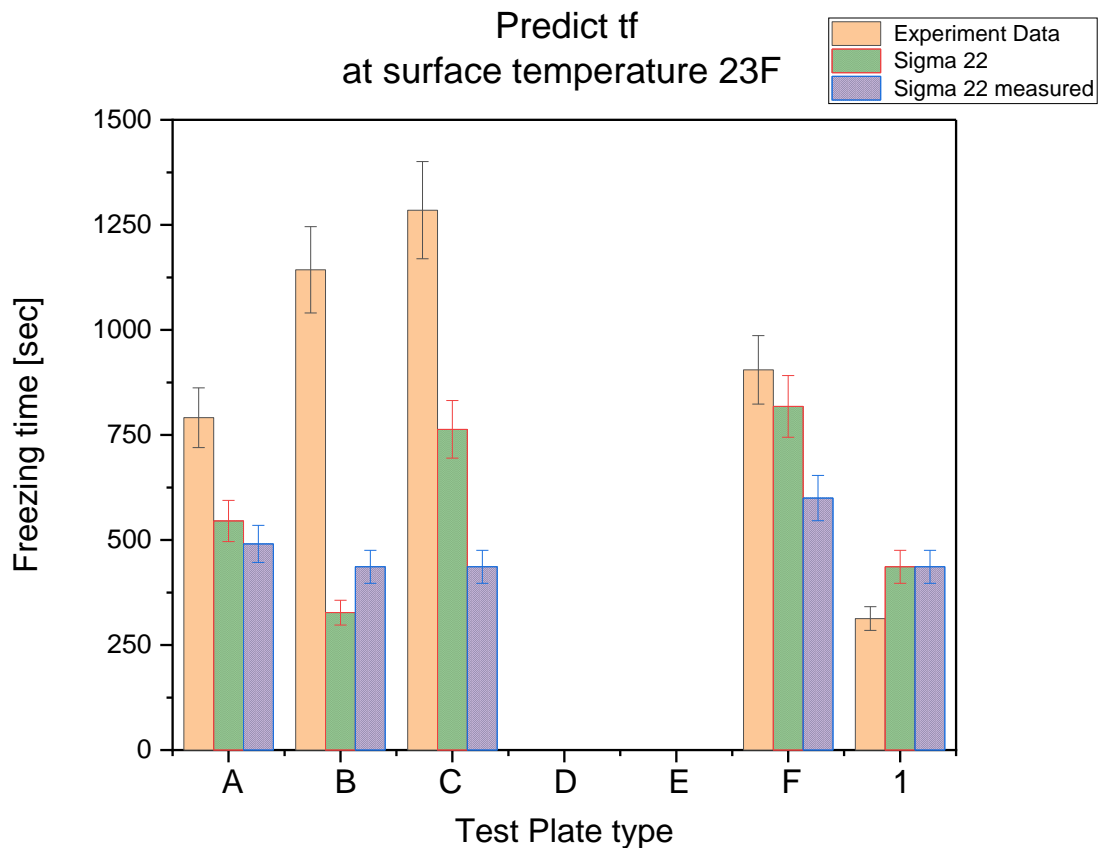


Figure 7.2: Predict freezing time of different surface wettability comparing the experiment test data at plate temperature 23 F (constant $F = 1e+12$).

The surface temperature 23F° model uses the same Cf factor (1-30) as the surface temperature 25° model. The nucleation rate at 23 F° is larger than 25 F° with the same surface tension of 22. That is the reason it has lower predicted freezing time. For these two-plot figures, surface tension σ varies from 26 to 19, but 22 is closer to experiment result based on Pure Aluminum plate 1. In Figure 7.2, there are not any repeat tests of plate D and plate E proceeded in these tests, so plate D and plate E are excluded in this comparison. Except super hydrophilic plate B, all other test plate predicted results are consistent with the actual experimental data. At lower surface temperature, the nucleation rate is increasing. Therefore, the predicted freezing time will be lower than 25°.

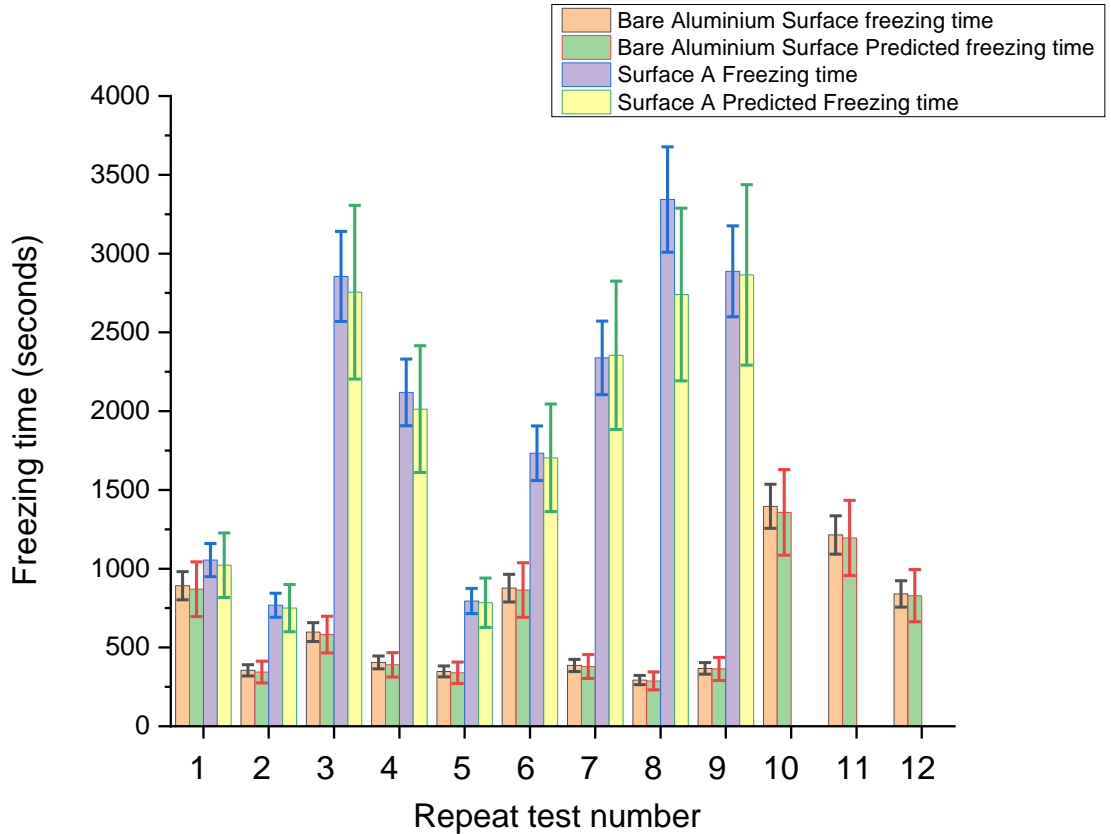


Figure 7.3: Predicted Freezing time of two different test plate with the more than 10 repeat tests with a certain assumed Cf factor range of (35-102) at 25 °F surface temperature, (constant F = 1e+12).

7.2 Comparison of modeling results with data from the literature

Predicted freezing time could be achieved by well developed modeling work in the previous study. These different model results would give a convience for proving the relevant parameters of predicting actual freezing time or freezing delay time. A new correlation was developed using data for cleaned surfaces from the current study, data from Bryant (1995), and five data points from Kim et al. (2016), which had relatively high surface temperatures and low supersaturation degrees. It was discovered that freezing time had different dependencies for this subset of experimental conditions than for lower surface

temperatures. For high surface temperatures, air velocity and the difference between the triple point and the surface temperature both strongly affected the freezing time, while these variables had minor effects on freezing time for data with low surface temperatures. The poor predictions were likely because Bryant's correlation was developed only for his data set. The temperature of the cold surface was always at $-10\text{ }^{\circ}\text{C}$, and it appeared that Bryant's correlation was not intended to be used for other surface temperatures. Kim et al (2016) described the freezing delay time for 100 sessile water droplets on bare and superhydrophobic surfaces. Random distribution of freezing delay times was reported in the range of 50-400s on bare surface and 100-1250s on superhydrophobic surface (153°) at the surface temperature of $-6.5\text{ }^{\circ}\text{C}$. They also applied the Fletcher modeled Gibbs energy barrier of heterogeneous nucleation of supercooled water droplet ΔG_{het} as their supported correlation to explain the random freezing time.

Several images also reported in their paper showed the nuclei growth process from the moment when the ice nuclei were first formed (set as 0 ms) in a water droplet. The nuclei growth process was recorded with the frame rate of 60 frame/s. The nuclei growth and ice crystal growth were similar to the concept of ice embryo nucleation in my dissertation. These clear images from Kim et al (2016) could provide a strong visual agreement with the ice embryo growth inside of water droplet until reaching the Gibbs energy barrier to have a phase change. In each water droplet freezing process, the embedded thermocouple still had a chance to give the path of fine contamination particles with the ice embryo. Although most locations of initial ice nucleation were not formed around the end side of the thermocouple, the contamination particles have been already

affecting the freezing delay time. In order to compare the experimental data from the literature with my model freezing time prediction results, the next figure 7.4 is presented.

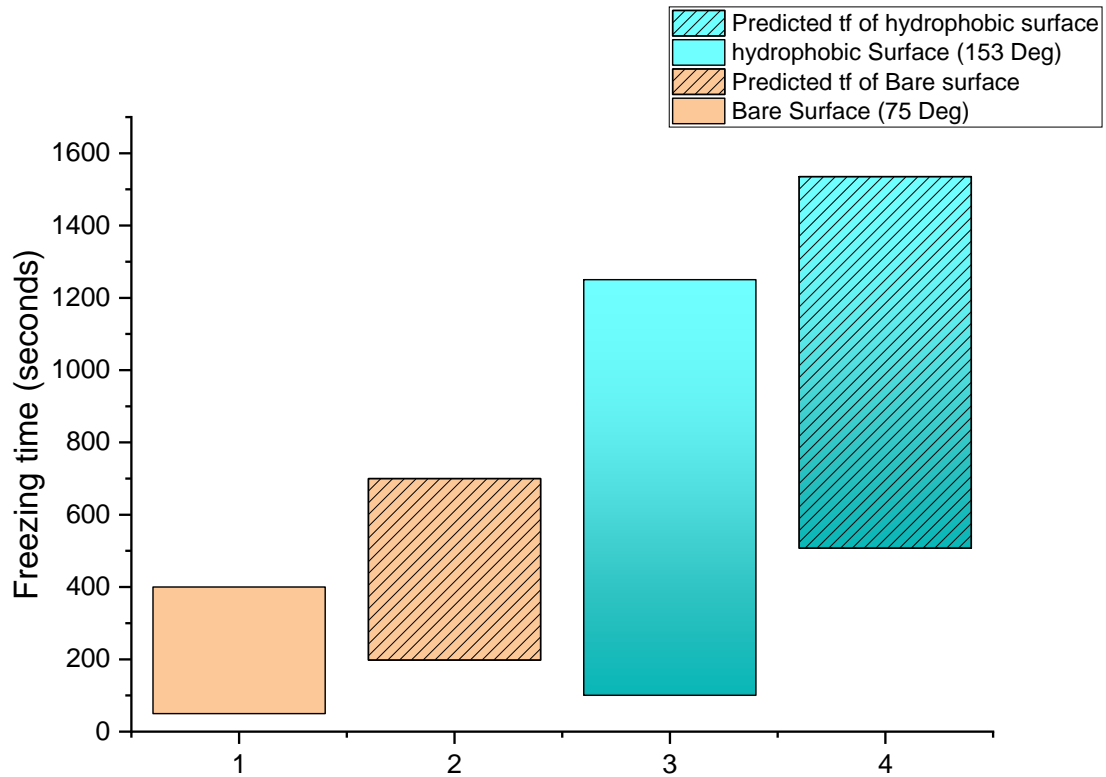


Figure 7.4: literature data validation with prediction results of two different contact angle surface at -6.5°C water droplet temperature.

In figure 7.4, Kim et al (2016) group reported the freezing delay time varies from 50-400s on bare surface and 100-1250s on superhydrophobic surface. The predicted tf resulted in columns 2 and 3 of two surfaces were estimated from the contamination model in this thesis. The uncertainty of freezing delay results was much different. Comparing the Bare surface, the freezing delay time of superhydrophobic surface had a large random range and uncertainty. The same prediction results of my model also showed that the large

range of freezing time in superhydrophobic surface. At -6.5°C subcooled temperature, the adjust factor F was equal to 10. The combination C_f factor of Bare surface prediction (column 2) was 7, while the combine C_f factor of superhydrophobic surface prediction (column 4) was 4. Combine C_f factor 7 and 4 resulted in the lowest freezing time and Combine C_f factor ($C_f = 1$) provided the longest freezing delay time because the homogeneous case ($C_f = 1$) was not dependent on the surface wettability.

The size of water droplets were different from my experiment data. The sessile water in Kim et al. work looked much bigger compared to the thermocouple as the reference. In my experiments, the water droplet was formed under forced convection and continuing wet air flow. The maximum size of water droplet formed in the cold plate was 0.5 mm more or less during the experiment observations. Because the water droplet size and air condition were different with Kim's group, considering the nitrogen gas might be trapped in the test chamber for couple minutes, the adjusted factor F selected from 1-10 under -6.5°C was considered a good assumption for my experimental data and Kim's research results.

Yao et al (2020) investigated the freezing process of water droplets based on local ice fraction. In many repeated experiment tests, at -10°C and -15°C , the water droplets on surface may still stay in supercooled liquid phase for long time (more than 10h) and unfreezing. The second phenomenon they observed was when surface temperature decreased to -18°C , -20°C , -22°C , -24°C and -26°C , the water droplets remained in supercooled state for a certain time until freezing process occurred. The ice fraction of single water droplets also was clearly showed in their supercooled liquid phase. Based on

their experiment results, the contamination model was applied again to compare the prediction freezing time.

Yao et al (2020) reported 32.8s, 22.2s, 16.7s, 11.4s, and 7.4s as the freezing delay time at different cold surface temperature of -18°C, -20 °C, -22 °C, -24 °C and -26 °C. Unfreezing time was found at -10 °C and -15 °C.

At surface temperature -20 °C, the contamination factor model predicted the freezing delay time is 21.1 seconds. The corresponding Cf factor used is 1 (homogeneous nuclei) and adjust factor constant F equals 1e+16. When Cf factor increased to 10 (heterogeneous case), the predicted freezing delay time would be 1.1 seconds and adjust factor constant F equals 1e+16 as the same. Thus, at a much lower supercooled temperature state, the F becomes in large value no matter Cf factor varies from homogeneous to heterogeneous. Looks like the ice nuclei rate would dominate the freezing time again. At higher surface temperature which closer to freezing point 0 °C, the contamination factor varied between 1 and 30, and it affected the freezing time. It also resulted in a larger uncertainty range comparing lower surface temperatures.

Although previous researchers provided many models to predict the actual freezing time, there are no contamination effect scenarios included in their models. The combine Cf model could fill this gap and well predict the uncertainty conditions and inconsistent freezing time.

7. 3 Model results for other common scenarios

Predicting the actual freezing time of different contact angles under two surface temperatures was shown in this model. Most predicted results were well matched with the

experiment data except the specific test plate. Applying the contamination factor to find the critical radius for each surface will become the key to predict the freezing time if frost nucleation rate is known. As we known, two surface temperature 25 F° and 23 F° has its own nucleation rate and the same constant Cf value, it could predict the most experiment freezing time data. But there are still limitations for predicting the actual freezing time when the Cf factor and surface temperature both affect the freezing time results. Thus, the first scenarios for predicting freezing time results surface temperature effects. When the surface temperature is high, many contamination particles would decrease the critical radius of the ice embryo and increase the speed of the frosting time; when the surface temperature is much lower like -40 C°, the contamination particles would not easily affect the free Gibbs energy to faster the freezing even high-level contamination particles added. In order to prove this scenario, the next following approaches need to be done. At the higher surface temperature 25 °F condition, varies the contamination factor 15% up and 15% down to see if it still could predict the freezing time for all the test plates. In the contract, at the lower surface temperature -4 °F, increasing or decreasing the contamination levels could not affect the actual freezing time too much. See Figure 7.31,

In this comparison the surface temperature has three levels, the first surface temperature is -3.8 °C (25°F). the second surface temperature for comparison is -40 °C (-40°F). Each surface temperature had its unique freezing time range at certain contamination level. At high surface temperature the critical radius of ice embryo is far away compared to the lower surface temperature. Varying the contamination factor between 10-30, critical radius of ice embryo is more clear and smaller than ice embryo size occurred at the higher

surface temperature. In order to accelerate the freezing process at the higher surface temperature, larger contamination factor range might be applied.

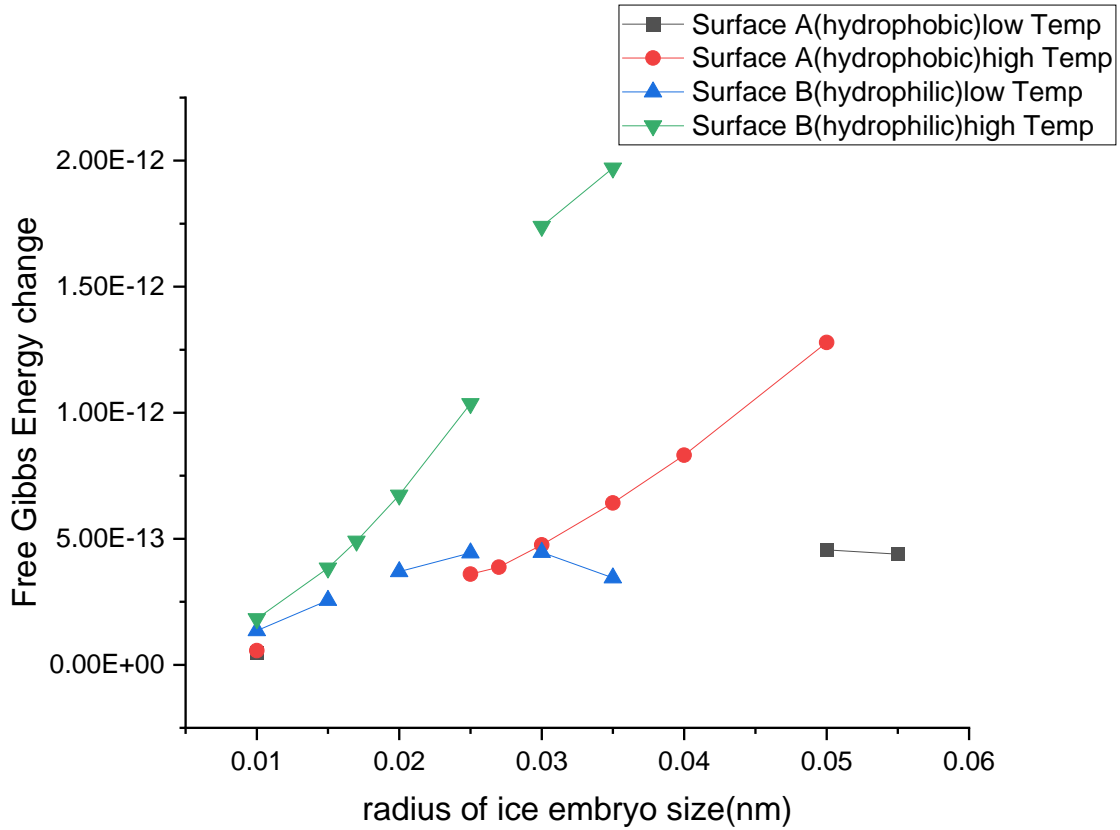


Figure 7.5: Free Gibbs energy change varies with radius of ice embryo under different subcooling temperature.

The second scenario for this predicting freezing time model is about the different contact angle surface may have the same predicting freezing time. This scenario phenomenon might be determined by the combined Cf factor and water droplets size in the early condensation stage. Normally at the same surface temperature test condition, super hydrophilic surface has low contact angle (less than 10°) and high combined Cf factor, the super hydrophobic surface has high contact angle (110 °) and lower combined Cf factor.

The onset freezing time prediction was calculated on critical radius size conditions. If the contamination particles applied on the early water condensation stage, when the water droplets are both extremely small on two different contact angle test plate, they may have the same water droplet radius and water droplet shape. At that moment, from the schematic of the water droplet on the cold test plate, the portion volume or area exposed to the air might be similar for different surface wettability. Another word to explain this inconsistent prediction freezing time, the portion volume or area of the water droplets exposed to the air may have the total same air contaminations effects for different test cold plate until droplets grows into the obviously wettability shape. To prove this scenario, two water droplets schematic are shown below, at the two different test plates and different test condition, the tiny water embryos or water droplets seeds may have same shape before growing completely. At this scenario, they may experience the same combined Cf and same nucleation rate to change the final freezing results. This scenario could give more uncertainty of the freezing time or unfreezing time. Also, the inconsistent freezing time results would occur if the water embryos or water droplets seeds didn't grow as their original path or growth trend.



Figure 7.6: at different periods, water droplets contact angle has no consistent measurement.

For test plate C, four measurements are 76.5, 58.2, 73.1, 75.4, thus the average of Plate C is 70.8 which is much closer to Test Plate B.

7.4 Summary of the findings and lesson learnt from modeling efforts.

The freezing process can be divided into five processes: (1) liquid cooling (supercooling), (2) nucleation, (3) recalescence, (4) freezing, and (5) solid cooling. In fact, the sudden changes of droplet volume and physical properties, especially the latent heat caused by the supercooling effect at the nucleation/recalescence stage, may significantly alter the freezing rate and the freezing time. The water-ice mixture has a smaller latent heat than the water, which accelerates the freezing process. The freezing rate and freezing duration time are critical points for the ice accretion prediction. Many researchers developed a completed test on a large diameter of droplet profiles, including the temperature and volume of the droplets for predicting the latent heat release during the freezing process. However, there is no correlation for tiny size water droplets or group droplets during the freezing process. There is a missing part from the literature about the effect of nearby droplets releasing latent heat to the next successive droplets.

From the literature, there is a classic nucleation theory to explain the water droplet suspended in the air will condense at the cold plate at certain conditions. Many researchers use thermocouples to measure the temperature of the water droplets and ice layers. Because the thermocouples were embedded in the liquid droplets to accelerate the freezing, Installed an infrared thermal camera above the surface and recorded the temperature change and captured the phase change process from liquid to solid. The infrared thermal camera measured both the temperature and the diameter of the droplets; thus providing estimates

of the water droplet surface coverage area and droplets diameter growth rate. Mass and volume of the frost were also measured by the experimental setup. Thus, with the density and thickness of the frost layer growth, the emissivity of the frost could be estimated at various temperatures. By using a calibration method to calculate the thermal conductivity of the frost layer with different test condition and different surface wettability, a final correlation of the thermal conductivity as function of emissivity, thickness, and temperature was developed. This correlation was used when analyzing the images from the IR camera to derive a meaningful surface temperature of the frost across the entire plate. Predicting the variability of the freezing time with the level of contamination of the surface is significant for many applications. Although researchers developed predicting freezing time methods, the contamination in the air and on the top of the test surface was usually neglected. Applying a slightly modified classic nucleation theory combined with the contamination factor predicted the actual freezing time and supported my experimental observations of recording significantly different freezing times for a flat surface exposed to the same frosting conditions. In layman terms, if the surface temperature, heat flux, air temperature, humidity, and speed are constant, how could the freezing time vary by as much as an order of magnitude? What was causing this randomly appearing freezing time of the flat plate? And is this phenomenon trackable and predictable? These are the questions that my dissertation addressed. When considering the level of contamination, my new semi-empirical theoretical thermodynamic model was able to explain how the presence of small particulate contaminants in the air can affect the mode of frost nucleation (homogenous vs. heterogenous) and the speed of freezing of the water droplets on the cold flat plates.

The different surface energy will have different water droplet shapes and sizes on the cold test plate. It also decided the water droplets wet area distribution on the entire test plate. What is more, the surface wettability will cause the water droplets to have a different growth rate. These exciting phenomena would lead to the water droplets on the cold test plate had different or inconsistent freezing time results. From the water-ice physic theory side, the different phases of droplets had different interfacial energy and density. The uncertainty of the freezing time of superhydrophobic surfaces is considerable. At the same continue test condition, there exists a large number of inconsistent freezing results and unfreezing. So we believe there must be a theory to support this interesting experiment phenomenon. Besides, we also found when the surface temperature was decreased from 25°F to 23°F, the uncertainty of the freezing time of each test became much smaller. From the literature review, Researchers analyzed the average test results with different contact angle surfaces. They had different models to predict the free Gibb energy change and average freezing time with different wettability surfaces. However, there is no strong relation to predicting the uncertainty of freezing time at the same test condition.

Chapter 8--Conclusion and lessons learnt.

Heat humps are widely used for efficient cooling and dehumidifying as well as winter heating. Frosting formation frequently occurs in the fin located on the evaporator of heat pump to slow down the heat removal and restrain the fullest cooling efficiency. Preventing frost formation will become a crucial task for generating new type air-source heat pumps or refrigeration systems. Understanding the frost formation or onset freezing characteristics will make it easier to create a new technique for developing high efficiency heat humps which could apply in complex outdoor environment.

Researchers did many experiment tests to investigate the frost nucleation phenomenon. As we known, the water condensation on cold test plate or frost/ice nucleation are highly influenced by air temperature, air humidity, air face velocity, droplet temperature and surface wettability. Many researchers also developed early droplet condensation model and crystal frost formation model. However, few researchers developed the model on different coating test plate, which the hydrophilic, hydrophobic and biophilic surface shows the contact angle and surface tension plays an important role in onset freezing or early nucleation phenomenon.

Air conditions and surface conditions both affect the water droplet distribution and frost nucleation on the cold test plate. Contamination particles suspended in the air and contamination particles on the top surface of the test plate can influence the frost embryo formation and growth. No matter the natural convection test or force convection test, there are different contamination levels affecting the nucleation results. However, there is a significant gap in characterizing the contamination level in the previous experimental and

theoretical studies. The common practice is to neglect the contamination level when predicting the nucleation rate. While this simplification could work reasonably well when predicting frost thickness on evaporators operating for a few hours, the contamination level could play an important role in the very initial few minutes of onset of frost nucleation. In addition, the freezing time can significantly be affected by the level of contamination of the frosting surface.

This dissertation presented a theoretical model that predicted the onset of frost nucleation on flat surfaces when surface energy and level of contamination were taken into consideration. The new model, which was also experimentally validated, captured the effects of surface contact angle and, more uniquely, isolated and quantified the effect of contamination of the surface in accelerating or delaying frost nucleation.

My Ph.D. research included experimental work and theoretical modeling and a summary of the conclusions for these two parts are summarized next.

Conclusions from the Experimental Work of this PhD Dissertation

The IR images of the present work showed that the static contact angle of the surface had a weak effect on the shape of the droplets before they turned into iced beads. For a similar contact angle of $\theta \approx 108^\circ$ to 110° , the substrate had a measurable effect on the droplet diameter when the surface temperature was at least 25°F or above. Hydrophobic surfaces investigated in the present work showed somewhat irregular splattered droplet shapes. This intriguing visual observation from the IR images appeared not consistent with the data shown in some literature studies (for example, in Harges et al. 2020). It might be due to differences in the specific surface coating chemistry and substrate materials of the flat plate investigated in the present work. Further investigations should be conducted in

future research before comparing the droplet shapes from surfaces with similar static contact angles with different chemistry of the coatings.

The different surface energy will have different water droplet shapes and sizes on the cold test plate. It also decided the water droplets wet area distribution on the entire test plate. What is more, the surface wettability will cause the water droplets to have a different growth rate. These exciting phenomena would lead to the water droplets on the cold test plate having different or inconsistent freezing time results. From the water-ice physics theory side, the different phases of droplets had different interfacial energy and density. The uncertainty of the freezing time of superhydrophobic surfaces is considerable. At the same continuous test condition, there exists a large number of inconsistent freezing results and unfreezing. So we believe there must be a theory to support this interesting experiment phenomenon. Besides, we also found when the surface temperature was decreased from 25°F to 23°F, the uncertainty of the freezing time of each test became much smaller. From the literature review, Researchers analyzed the average test results with different contact angle surfaces. They had different models to predict the free Gibbs energy change and average freezing time with different wettability surfaces. However, there is no strong relation to predicting the uncertainty of freezing time at the same test condition.

Conclusions from the Modeling Work of this PhD Dissertation

Early frost nucleation and frost growth are always the popular topic for many researchers investigated. Experimental tests will give the most intuitive frost results which include water droplets size, water droplets distribution, droplets shape, freezing time, frost height, frost density, frost formation rate or melting rate etc. These interesting frost experiment phenomena firstly was highly influenced by the air conditions in the wind

tunnel or outdoor environment. The air conditions could be briefly summaries as air face velocity, air temperature and moisture air humidity. Lower air temperatures or higher air humidity ratio could faster the water droplets nucleation and onset freezing. The air face velocity not just changes the freezing time but also could change the water nucleation size or wet area distribution on the test plate. The second factor could influence the frost characteristic is the surface conditions which include the surface temperature and surface wettability. Although researchers did many experiments test to analyze the surface wettability from lower contact angle to higher contact angle conditions, there is too less targeted test on contamination particles effect on the frost results. In this dissertation research, contamination particles suspended in the air or attached on the top surface of the cold plate can influence the frost nucleation rate and surface wettability condition. Normally the any contamination particles could directly shorten the actual freezing time because the internal energy or chemical reaction changed the original freezing process or growth path. To dig out the theory which support this nucleation phenomena, different cleaning method test and continually repeat frost test were proceeded to provide evidential freezing or unfreezing experimental data.

In this dissertation, except for large quantity frost test under different test condition and different surface wettability, Contamination factor combine with the Classical Nucleation Theory (CNT) will be introduced to predict the actual freezing time and explain the unfreezing or inconsistent freezing phenomena during repeat frost tests.

In this model, contamination particles size was assumed based on the air filter of the wind tunnel which had PM2.5. With certain amounts of assumptions of parameters, different model work will be used to analyze these plenty experimental raw data. The first model is

inserting varies contamination factor in the critical Gibbs energy equation to find the critical radius of the ice embryo in the water droplets. The critical size of ice embryo could directly illustrate the time used to reach the maximum Gibbs energy barrier for each single droplet is getting shorter when contamination level increased. The second model is different contact angle will become the key to make the critical free Gibbs energy transfer from homogeneous model to heterogeneous model. The f function will be introduced again and combined with the new concept that contamination factor to emphasize importance of the contact angle in second model. The third model is not just considering the contaminations from the air, the substrate surface contamination particles could still change the surface wettability and accelerate the freezing time. Using the water droplets schematic on the top surface of the test plate. One portion of the water droplet is exposed to the air and the rest of the droplet is attached to the substrate surface in this schematic if spherical shape was assumed. The portion volume ratio or area ratio will give a combination of the air contamination and the substrate contamination factors. However, lower contact angle to higher contact angle will distinguish which portion was heavily influenced by air or substrate condition. Frost nucleation rate will be calculated for each test plate to apply the prediction of actual freezing time. The combine contamination model will give a second chance to recalculate the nucleation rate to predict the freezing time. This novelty section in this model will well filled up the missing part in the literature.

Overall final thoughts.

Although many experiment tests were finished to investigate the air condition and surface condition sensitive parameters, there are lots of lessons learnt during experiments. Firstly,

in order to maintain the same input of the repeat frost test, such as same air humidity and same substrate temperature, the steady state test is necessary to check the substrate installation and same experiment condition for next frost test. Secondly, after each frost test, cleaning different test substrate surface should be gently treated. Because the top surface has a chemical coating and is easily destroyed or worn out during the long-time repeatable testing. Using isopropyl alcohol and deionized water to clean the top surface will be applied in this series of repeat tests. There are still lots of points which is undiscovered during the experiment test or modeling work. Revising the C_f factor model would make it easier to understand the ice nucleation theory. It also help to improve the precision of freezing time prediction for all different conditions.

Chapter 9--Future Work

For future addition work in this dissertation and research, there are still lots of technical sections that need to be upgraded. Here are some suggestions for next actions for improving this modeling work and dissertation incomplete part. Firstly, the assumption of contamination particles size can be improved to be more precise. For example, the Cf factor range could be changed from 1 to 2000. Besides, the surface contamination particles size can be assumed to be accurate when it was trying to match with the actual substrate surface roughness and contact angle pitches space structure. Because these contamination particles no matter in the air or substrate, they will become the powerful factor to accelerate the freezing time. Also, from the experiment side, there is no clear video record in the very early period to capture the contamination particles affect the water nucleation seeds growth. Additional camera tools need to be applied in future work to experience a better testing environment. The second improvement is the top surface of the substrate had many contamination particles which couldn't recognized by naked eyes or thermal camera after each frost test. These extremely tiny particles attached inside of the contact angle pitches room need to be well measured by high resolution camera. The possible approach to measure the contamination particles or contact angle is 3D scanning method. Besides, the third suggestion for the future work is about the predicting model. Due to the limitations of this model, the same surface wettability conditions will have the same volume ratio distribution from portion above surface to below surface. Thus, the predicted freezing time will be same when two test plates have the same contact angle because combined Cf factor will change the ice embryo critical size and growth rate. Two approaches could solve this limitation and improve the precise of predicting. One is the chemical reaction within the

water droplets that need to be considered. Clear water molecules and ice embryos may have chemical reactions to become a new product which is the ice crystal structure. In this dissertation work, only contamination particles inserted into the reaction equation as the input. The chemical coating element of the top substrate and contamination particles could still be considered to react with the ice/water embryo molecules groups. That might be a new studied direction for the future work. Another approach could be applied to improve the current work and have better prediction is knowing the specific free Gibbs energy during each freezing process. Because in the current research model, the freezing time was predicted by using the time from single water molecules grew up to the critical size which means reach the maximum energy barrier. Sometime, the nucleation rate was super large for calculating the small water droplet size. The adjusted factor must be applied to make the calculating results more reasonable. If using the time when free Gibbs energy value equal to zero increased to the maximum number, the prediction results might be more precise. In the last, it is worth to expect the more efficient method could be developed in the future work.

Reference

- Hoke, J.L., Georgiadis, J.G., Jacobi, A.M., 2000. *The interaction between the substrate and frost layer through condensate distribution*. Air Conditioning and Refrigeration Center. College of Engineering. The University of Illinois at Urbana-Champaign.
- Tao, Y.-X., Besant, R. W., Mao, Y., 1993. “Characteristics of frost growth on a flat plate during the early growth period.” *ASHRAE Transactions* 99, pp. 746-753.
- Byeongchul Na., Ralph L. Webb., 2003 “A fundamental understanding of factors affecting frost nucleation” *International Journal of Heat and Mass Transfer* Volume46, Issue 20, pages 3797-3808
- Wei Sheng, Yang Pei, Xueli Li, Pingmei Ming, Weilong Zhao, 2020. “Effect of surface characteristics on condensate droplets growth”, *Applied Thermal Engineering*, Volume 173, 115260,
- Hyunsik Kim, Youngsuk Nam,2016. “Condensation behaviors and resulting heat transfer performance of nano-engineered copper surfaces”, *International Journal of Heat and Mass Transfer*, Volume 93, Pages 286-292,
- Seki, N., Fukusako, S., Matsuo, K., Uemura, S., 1985. An analysis of incipient frost formation. *Wärme-und Stoffübertragung* 19(1), pp.9-18.
- Bryant, J., 1995. *Effects of hydrophobic surface treatments on dropwise condensation and freezing of water*. Doctoral dissertation, Texas A&M University.
- Adanur, B., 2019. *Experimental methods for the analysis of frost nucleation and frost growth on hydrophilic and hydrophobic coated flat plate surfaces in forced convection channel flows*. Master’s thesis, Auburn University, Auburn, AL, USA.
- Adanur, B., Cremaschi, L., Harges, E., 2019. “Effect of mixed hydrophilic and hydrophobic surface coatings on droplets freezing and subsequent frost growth during air forced convection channel flows.” *Science and Technology for the Built Environment* 25(10), pp. 1302-1312.

- Harges, E., Cremaschi, L., Adanur, B., 2019. “A new model for droplets growth during their onset of freezing on flat surfaces under air forced convection.” *Proceedings of the 25th IIR International Congress of Refrigeration*, Montreal, Canada. Paper 569.
- Donghee Kim, Hisuk Kim, Sun Woo Kim, Dong Rip Kim, Kwan-Soo Lee, 2015, “Experimental investigation of frost retardation for superhydrophobic surface using a luminance meter”, *International Journal of Heat and Mass Transfer*, Volume 87, Pages 491-496.
- Şahin, A. Z. 1995. An analytical study of frost nucleation and growth during the crystal growth period. *Heat and Mass Transfer* 30(5), pp. 321-330.
- Sommers, A. D., Napora, A. C., Truster, N. L., Caraballo, E. J., Hermes, C. J., 2017. A semi-empirical correlation for predicting the frost density on hydrophilic and hydrophobic substrates. *International Journal of Refrigeration* 74, pp. 313-323.
- Piucco, R.O., Hermes, C.J., Melo, C., Barbosa Jr, J.R., 2008. A study of frost nucleation on flat surfaces. *Experimental Thermal and Fluid Science* 32(8), pp.1710-1715.
- Xian-Min Guo, Yi-Guang Chen, Wei-Hua Wang, Chun-Zheng Chen, 2008. “Experimental study on frost growth and dynamic performance of air source heat pump system”, *Applied Thermal Engineering*, Volume 28, Issues 17–18, Pages 2267-2278,
- Yoong Chung, Jin Woo Yoo, Gwi Taek Kim, Min Soo Kim, 2019, “Prediction of the frost growth and performance change of air source heat pump system under various frosting conditions”, *Applied Thermal Engineering*, Volume 147, Pages 410-420,
- Bo Xu, Qing Han, Jiangping Chen, Feng Li, Nianjie Wang, Dong Li, Xiaoyong Pan, 2013, “Experimental investigation of frost and defrost performance of microchannel heat exchangers for heat pump systems”, *Applied Energy*, Volume 103, Pages 180-188,
- Shao, L., Yang, L., & Zhang, C. (2010). Comparison of heat pump performance using fin-and-tube and microchannel heat exchangers under frost conditions. *Applied Energy*, 87, 1187-1197.

- Y. Xia, Y. Zhong, P.S. Hrnjak, A.M. Jacobi, 2006, “Frost, defrost, and refrost and its impact on the air-side thermal-hydraulic performance of louvered-fin, flat-tube heat exchangers”, *International Journal of Refrigeration*, Volume 29, Issue 7, Pages 1066-1079,
- Aurélia Leoni, Michèle Mondot, François Durier, Rémi Revellin, Philippe Haberschill, 2017, “Frost formation and development on flat plate: Experimental investigation and comparison to predictive methods”, *Experimental Thermal and Fluid Science*, Volume 88, Pages 220-233,
- Christian J.L. Hermes, Robson O. Piucco, Jader R. Barbosa, Cláudio Melo, 2009, “A study of frost growth and densification on flat surfaces”, *Experimental Thermal and Fluid Science*, Volume 33, Issue 2, Pages 371-379,
- Shinhyuk Yoon, Gaku Hayase & Keumnam Cho (2010) Measurements of Frost Thickness and Frost Mass on a Flat Plate under Heat Pump Condition, *Heat Transfer Engineering*, 31:12, 965-972, DOI: [10.1080/01457631003638911](https://doi.org/10.1080/01457631003638911)
- Yanhui Mao, 1991, “The measurement and analysis of frost accumulation on a flat plate with forced convection” Harvest, Graduate Theses and Dissertations.
- Sheng, W., Pei, Y., Li, X., Ming, P., Zhao, W., 2020. Effect of surface characteristics on condensate droplets growth. *Applied Thermal Engineering*, p.115260.
- Kim, H., Kim, D., Jang, H., Kim, D.R., Lee, K.S., 2016. Microscopic observation of frost behaviors at the early stage of frost formation on hydrophobic surfaces. *International Journal of Heat and Mass Transfer* 97, pp.861-867.
- Hoke, J.L., Georgiadis, J.G., Jacobi, A.M., 2000. *The interaction between the substrate and frost layer through condensate distribution*. Air Conditioning and Refrigeration Center. College of Engineering. The University of Illinois at Urbana-Champaign.
- Seki, N., Fukusako, S., Matsuo, K., Uemura, S., 1985. An analysis of incipient frost formation. *Wärme-und Stoffübertragung* 19(1), pp.9-18.
- Bryant, J., 1995. *Effects of hydrophobic surface treatments on dropwise condensation and freezing of water*. Doctoral dissertation, Texas A&M University
- Hayashi, Y., Aoki, A., Adachi, S., Hori, K., 1977. Study of frost properties correlating with frost formation types. *Journal of Heat Transfer* 99, pp. 239-245.
- Max Kandula, 2011, “Frost growth and densification in laminar flow over flat surfaces, *International Journal of Heat and Mass Transfer*”, Volume 54, Issues 15–16, Pages 3719-3731,

- Dong-Keun Yang, Kwan-Soo Lee, 2004, "Dimensionless correlations of frost properties on a cold plate", *International Journal of Refrigeration*, Volume 27, Issue 1, Pages 89-96,
- Shin, J., Tikhonov, A. V., and Kim, C. (January 29, 2003). "Experimental Study on Frost Structure on Surfaces With Different Hydrophilicity: Density and Thermal Conductivity ." *ASME. J. Heat Transfer*. February 2003; 125(1): 84–94.
- Harges, E., Cremaschi, L., Adanur, B., 2020. Distribution, coalescence, and freezing characteristics of water droplets on surfaces with different wettabilities under subfreezing convective flow. *Applied Thermal Engineering* 182, 116052.
- J.M. Armengol, C.T. Salinas, J. Xamán, K.A.R. Ismail, 2016 "Modeling of frost formation over parallel cold plates considering a two-dimensional growth rate", *International Journal of Thermal Sciences*, 2016, Pages 245-256, ISSN 1290-0729,
- Moallem, Ehsan, et al. "Experimental measurements of the surface coating and water retention effects on frosting performance of microchannel heat exchangers for heat pump systems." *Experimental Thermal and Fluid Science* 39 (2012): 176-188.
- Cheng, Chin-Hsiang, and Keng-Hsien Wu. "Observations of early-stage frost formation on a cold plate in atmospheric air flow." *J. Heat Transfer* 125.1 (2003): 95-102.
- Yang, Dong-Keun, Kwan-Soo Lee, and Dong-Jin Cha. "Frost formation on a cold surface under turbulent flow." *International journal of refrigeration* 29.2 (2006): 164-169.
- Na, Byeongchul, and Ralph L. Webb. "A fundamental understanding of factors affecting frost nucleation." *International Journal of Heat and Mass Transfer* 46.20 (2003): 3797-3808.
- Yancheshme, A. A., Momen, G., & Aminabadi, R. J. (2020). Mechanisms of ice formation and propagation on superhydrophobic surfaces: A review. *Advances in Colloid and Interface Science*, 279, 102155.
- Marinyuk, B. T. (1980). Heat and mass transfer under frosting conditions. *International Journal of Refrigeration*, 3(6), 366-368.
- Lee, K. S., Kim, W. S., & Lee, T. H. (1997). A one-dimensional model for frost formation on a cold flat surface. *International Journal of Heat and Mass Transfer*, 40(18), 4359-4365.
- Şahin, A. Z. (1995). An analytical study of frost nucleation and growth during the crystal growth period. *Heat and Mass Transfer*, 30(5), 321-330.

- Yao, Y., Yang, R., Li, C., Tao, Z., & Zhang, H. (2020). Investigation of the freezing process of water droplets based on average and local initial ice fraction. *Experimental Heat Transfer*, 33(3), 197-209.
- Kim, M. H., Kim, D. R., & Lee, K. S. (2017). Stochastic approach to the anti-freezing behaviors of superhydrophobic surfaces. *International Journal of Heat and Mass Transfer*, 106, 841-846.
- Min-Hwan Kim, Dong Rip Kim, Kwan-Soo Lee, 2017, “Stochastic approach to the anti-freezing behaviors of superhydrophobic surfaces”, *International Journal of Heat and Mass Transfer*, Volume 106, Pages 841-846,
- Julian E. Castillo, Yanbo Huang, Zhenhai Pan, Justin A. Weibel, 2021, “Quantifying the Pathways of Latent Heat Dissipation during Droplet Freezing on Cooled Substrates”, *International Journal of Heat and Mass Transfer*, Volume 164, 120608,
- Victor Voulgaropoulos, Mohammadreza Kadivar, Mohammad Ardekani Moghimi, Mohamed Maher, Hameed Alawadi, Omar K. Matar, Christos N. Markides, 2021, “A combined experimental and computational study of phase-change dynamics and flow inside a sessile water droplet freezing due to interfacial heat transfer”, *International Journal of Heat and Mass Transfer*, Volume 180, 121803,
- Xuan Zhang, Xiaomin Wu, Jingchun Min, Xin Liu, 2017, “Modelling of sessile water droplet shape evolution during freezing with consideration of supercooling effect”, *Applied Thermal Engineering*, Volume 125, Pages 644-651,
- Fuqiang Chu, Xiaomin Wu, Lingli Wang, 2017, “Dynamic Melting of Freezing Droplets on Ultraslippery Superhydrophobic surfaces” *ACS Applied Materials & Interfaces* 2017 9 (9), 8420-8425
- Jiaying Gong, Jinjuan Sun, Guojun Li, 2017 “An experimental study of the effect of air quality on frosting on cold flat surface”, *International Communications in Heat and Mass Transfer*, Volume 82, Pages 139-144,
- Blake, J., Thompson, D., Raps, D., & Strobl, T. (2015). Simulating the freezing of supercooled water droplets impacting a cooled substrate. *AIAA Journal*, 53(7), 1725-1739.
- Niedermeier, D., Shaw, R. A., Hartmann, S., Wex, H., Clauss, T., Voigtländer, J., & Stratmann, F. (2011). Heterogeneous ice nucleation: exploring the transition from stochastic to singular freezing behavior. *Atmospheric Chemistry and Physics*, 11(16), 8767-8775.

- Pruppacher, H. R. (1995). A new look at homogeneous ice nucleation in supercooled water drops. *Journal of Atmospheric Sciences*, 52(11), 1924-1933.
- Chaudhary, G., & Li, R. (2014). Freezing of water droplets on solid surfaces: An experimental and numerical study. *Experimental Thermal and Fluid Science*, 57, 86-93.
- Zhang, H., Zhao, Y., Lv, R., & Yang, C. (2016). Freezing of sessile water droplet for various contact angles. *International journal of thermal sciences*, 101, 59-67.
- O'Neal, D. L., & Tree, D. R. (1984). Measurement of frost growth and density in a parallel plate geometry. *Ashrae Transactions*, 90(2), 278-290.

Appendix

```



```

```

EXP = -(D_G_star/down)
I_1 = exp(EXP )
I = I_0 * I_1

%freezing time

r_water_molecule = 2*10^(-8);% r=0.2nm; unit 0.2 nm = (10^-8)cm
r_ice_embryo=80*r_water_molecule;
DT=40; % 40C
DS=(1.13-0.004*DT)*(10^7);% erg cm-3 deg-1
DG_v = -DS*DT;
%r=Cf*r_ice_embryo;
r=0.000000004 % Cf_air =2 the critical radius as the start point

sigma= 16;% because of contamination, sigma had a 30% reduction. unit:
erg cm-2
DG_r = (4*pi/3)*(r^3)*(DG_v)+(4*pi*(r^2)*sigma)
r_star=-2*sigma/DG_v% critical radius without contamination
DG_r_star = (4*pi/3)*(r_star^3)*(DG_v)+(4*pi*(r_star^2)*sigma)%without
contamination
DG_critical = [16*pi*sigma^3]/[3*(DG_v)^2];%without contamination;
r_star_C=Cf*r % with contamination factor Cf
DG_critical_C=(4*pi/3)*(r_star_C^3)*(DG_v)+(4*pi*(r_star_C^2)*sigma)%
with contamination factor Cf
%nucleation rate
D_G_star = DG_critical_C;
k = 1.38066*10^(-16); %[erg/K]
T_k=233.15; % K -40C %269.261@ 25F
down = k*T_k;
EXP = -(D_G_star/down);
I_1 = exp(EXP );
I_0=4.53999E+30;
I_calculate = I_0 * I_1
r_star_C_new = 0.045 %nm, not the cm.
I =3.23E+24/4.18879; %assumed nucleation rate cm-3 s-1
I_c = nthroot(I,3) % unit change to cm-1 s-1 === cube root of I
tf=((r_star_C_new-r_water_molecule)/I_c)*1e+12

```